Memoirs of the Faculty of Science, Kyoto University, Series of Physics, Astrophysics, Geophysics and Chemistry, Vol. XXXIX, No. 3, Article 3, 1996

Search for H dibaryon in $\Sigma^- p$ decay with scintillating fiber target as triggerable visual detector

By

Yoshitaka ITOW

Department of physics, Faculty of Science, Kyoto University
Kyoto 606-01, Japan

(Received November 22, 1995)

Abstract

A H dibaryon search via (K^-, K^+) reactions has been performed with a novel visual detector, scintillating fibers, as a triggerable active target using KEK 12-GeV Proton Synchrotron. The target is made of 30,000 plastic scintillating fibers and viewed by two sets of image intensifier tubes. The tracks are clearly identified as the images of photons in the pictures obtained with the image intensifier tubes. The position resolution of tracks has been obtained to be 290 μm. The target has been used for detecting three-dimensional images of (K^-, K^+) reactions and decay products of the H. The H dibaryon through the direct production process, $K^- + C \rightarrow K^+ + H + X$ followed by the sequential weak-decay, $H \rightarrow \Sigma^- + p$, then $\Sigma^- \rightarrow \pi^- + n$, has been searched in about 8,000 pictures of (K^-, K^+) reactions obtained with the target.

No evidence for the H has been observed. The upper limit for the production cross section of H has been obtained to be 0.35 μb to 0.5 μb for the H mass of 2200 to 2230 MeV/c^2 and the lifetime of 10^{-10} to 10^{-9} with assumption that the decay branching ratio for $\Sigma^- p$ channel is 100%.

1 Introduction

1.1 H dibaryon

In spite of the complex aspect of non-pertubative QCD, a simple picture of the naive quark-model of hadron, in which there are 3 quarks (qqq) in a baryon and quark-antiquark ($q\bar{q}$) in a meson, has been successful for describing the attributes of hadrons such as the charge, spin, and the magnetic moment.

An extension of the quark picture leads us to possible existence of multiquark states ($q^n\bar{q}^m$), so-called exotic hadrons. Both theoretical and experimental studies have been made on exotic hadrons [1].

A six quark state (q^6) was studied by Jaffe in the framework of the MIT-bag model in 1977 [2]. He proposed the existence of a flavor-singlet dihyperon ($uuddss$), the H dibaryon, which has strangeness -2 and is an iso-singlet ($I=0$) and spin-singlet ($J=0$) state. The predicted mass is 2150 MeV/c^2 so that the H is stable against strong decay into $\Lambda\Lambda$ ($2M_\Lambda = 2230$MeV/c^2). Such a large binding energy is originated in the "color magnetic interaction" due to the one-gluon exchage between quarks.

Since then, many papers have been devoted to calculate its mass with various models, such as the bag model [3, 4, 5], the quark cluster model [6, 7, 8], the skyrme

model [9, 10], the Lattice QCD [11] and so on. Many of these calculations suggest that the H is bound although predicted masses are scattered in wide range (1800 MeV/c^2 ~ 2Λ mass).

1.2 Experimental studies

Experimental studies have been made to search for the H in two ways. One is to search for the signal in the missing mass spectrum for the production channel. The other is direct detection of the decay products.

At BNL, the H was searched for in the missing mass spectrum of the reaction $p + p \rightarrow K^- + K^+ + H$. It gave an upper limit for the production cross section, 30-130 nb in the M_H range from 2000 MeV/c^2 to 2500 MeV/c^2 (90% C.L.) [12], whereas the expected production cross section [13] is two orders of magnitude smaller than the obtained limit.

Recently, observations of several weak-decay events of the H have been reported by a group from Dubna. A propane bubble chamber has been exposed to 10-GeV/c proton beams [14, 15]. They have claimed by means of a kinematically fitting method that neutral "Vee" particles have been intepreted as the H decaying into $\Sigma^- p$. Another experiment has shown the $H \rightarrow \Lambda p \pi^-$ decay in a spark chamber with a Cu target exposed to neutron beam [16]. There remains, however, other possible interpretations for these events [17]. The $H \rightarrow \Sigma^- p$ event can be faked by inelastic scattering of Λ such as $\Lambda + n \rightarrow \Sigma^- + p$. The $H \rightarrow \Lambda p \pi^-$ event can be faked by a two Λ production event where one of the Λ changes the direction by the elastic scattering. The identification of double strangeness transfer at the production point of H is indispensable to deny such interpretations.

Dover et al pointed out in 1982 [18, 19] that the (K^-, K^+) reaction on a nucleus target is a good channel for this purpose. In this reaction two production processes of the H are considered. One is the direct H production process;

$$K^- + (pp) \rightarrow K^+ + H, \tag{1}$$

where (pp) is a proton pair inside a nucleus. The other is the Ξ^- absorption process;

$$\Xi^- + (p) \rightarrow H + X, \tag{2}$$

where (p) is a proton in a nucleus. The Ξ^- produced via a (K^-, K^+) reaction is slowed down by ionization and is captured in an atomic orbit.

In 1989 an emulsion-counter hybrid experiment (KEK-E176) using the (K^-, K^+) reaction was performed at KEK. In this experiment, (K^-, K^+) interaction points were determined with a K^+ -spectrometer and Ξ^-'s produced at the first vertex were tagged. The H was searched in (K^-, K^+) reactions as well as in Ξ^- absoption reactions with the emulsion target. The signal of the direct H production via (K^-, K^+) reaction was searched in the K^+ momentum spectrum. The result gave an upper limit for the production cross section to be 0.2%-0.6% (90% C.L.) of the quasi-free Ξ^- production in the mass range of 1900 MeV/c^2-2160 MeV/c^2 [20]. The decay products of $H \rightarrow \Sigma^- p$ channel were also searched in the volume of 1 mm^3 around the Ξ^- absorption points in emulsion. No evidence of the H decay was found, and the

upper limit for the H production was deduced as 6% (90% C.L.) [21]. The result, however, was limited for the H with short life ($\leq 10^{-10}$sec) due to the small fiducial volume of the scanning. Therefore, the question is still open for the H with longer lifetime ($\geq 10^{-10}$sec).

Another information is derived from the studies of double Λ hyper-nuclei. In KEK-E176, a few cascade weak decays of double Λ hyper-nuclei were found in about 100 candidates of Ξ^- absorption at rest in emulsion [22]. One of the events was determined as either ${}_{\Lambda\Lambda}^{10}Be$ or ${}_{\Lambda\Lambda}^{13}B$. The binding energy of 2 Λ ($B_{\Lambda\Lambda}$) was determined to be 8.5 $\pm$ 0.7 MeV for ${}_{\Lambda\Lambda}^{13}Be$ or 27.6 $\pm$ 0.7 MeV for ${}_{\Lambda\Lambda}^{13}B$. If the H mass is less than 2Λ mass, the transition ${}_{\Lambda\Lambda}^{A}Z \rightarrow H + {}^{A-2}Z$ takes place through the strong interaction. Thus the lower limit of the H mass might be deduced to be 2203.7 $\pm$ 0.7 MeV/c^2 from the larger $B_{\Lambda\Lambda}$. However, the possibility is still open for the H heavier than 2200 MeV/c^2. There has been, so far, no definite answer to its existence.

1.3 Motivation of the present experiment

Although the nuclear emulsion method has a very high spatial resolution ($\sim 1\,\mu$m), the effective volume to search for weak-decay products of neutral particles is limited within 1 mm^3, and the number of exposed beam particles is limited since it has no time resolution. The limits in previous experiments can be overcome by a counter hybrid technique together with a novel active target which has a large effective volume and a good time resolution.

Recently, scintillating fiber detectors have been developed for high-resolution trackers [24, 25, 26, 27] and active targets [28, 29, 30, 31] for high-energy physics experiments.

We have developed a new type of visual detector, SCIFI-target, which has worked as a triggerable active target, utilizing plastic scintillating fibers and image intensifier tubes [32]. The present experiment (KEK-E224) has been planned using this detector to obtain pure (K^-, K^+) reactions with higher statistics than the previous experiments and to search for the H both via the direct process shown in Eq. 1 and via the Ξ^- absorption process as shown in Eq. 2 by observing its decay products such as $H \rightarrow \Sigma^- p$.

This detector can provide visual image of (K^-, K^+) reactions, the following secondary interactions and the decay products. Because of fast gating operation, most of the tracks due to background reactions have been eliminated in the picture. Therefore, it is easy to identify a neutral particle from its decay mode. These unique advantages of the SCIFI-target provide us a new method for studying of the H dibaryon, and open a new field of hyperon physics at intermediate energy region.

In this paper we focus on the study of the direct H production in the mass range from 2200 to 2230 MeV/c^2 by means of the observation of the decay products in the SCIFI-target. Since the direct H production is a quasi-free reaction, a possible signal of H production can be identified as a peak in the K^+ momentum spectra in the reaction shown in Eq. 1. For heavier H mass of interest, however, the peak corresponding to the H production is hardly separated from a large tail of the quasi-

free Ξ^- production process in the K^+ momentum spectrum. Therefore, the existence of the H could be examined by means of the observation of its decay products in the pictures obtained with the SCIFI-target. The H has been identified as the weak decay sequence;

$$H \rightarrow \Sigma^- + p, \quad \text{then} \quad \Sigma^- \rightarrow \pi^- + n. \tag{3}$$

The present experiment was performed at the K2 beam line in KEK 12-GeV Proton Synchrotron. The SCIFI-target was exposed to 1.66-GeV/c K^- beam with the intensity of 2×10^4/spill. The momenta and velocities of the incident and scattered particles were analyzed with high resolution spectrometers both upstream and downstream of the target. Using information from the spectrometers, the double strangeness transfer at the first vertex were confirmed. Thus only the data on (K^-, K^+) reactions in the SCIFI-target have been analyzed. About 8,000 pictures of (K^-, K^+) reaction have beeen collected and analyzed to search for the H.

The experimental setup is presented in Section 2. In Section 3 we describe the SCIFI-target in detail, including the data handling method and the basic performance of the SCIFI-target. We describe the procedure for the analysis of the direct H production search in Section 4. The results and discussions are given in Section 5. The conclusion is given in Section 6.

2 Experimental setup

We briefly summarize our experimental setup except the SCIFI-target, which is described in Section 3.

2.1 KEK K2 beam line

The experiment was performed at the K2 beam line in KEK 12-GeV Proton Synchrotron (PS). The specification of the K2 beam line is listed in Table 1. Primary protons were extracted from the PS during two seconds after every two seconds of acceleration cycle, and transported to the primary target point of the K2 beam line. A schematic view of the K2 beam line is shown in Fig. 1. The K2 beam

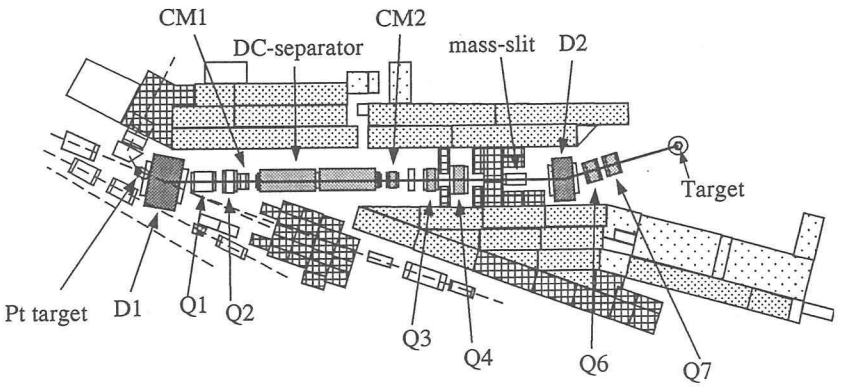

Fig. 1. The top view of the K2 beam line.

Table 1. The specification of the K2 beam line.

beam length	28.9 m
primary target	platinum(6 mm×3 mm×60 mm)
production angle	0 degree
momentum range	1−2.1 GeV/c
angular acceptance	±50 mrad.(H)×±6.5 mrad.(V)
beam size(r.m.s.)	7.8 mm(H)×5.8 mm(V)
momentum byte	3.6%

line was designed to produce an enriched kaon beam with the momentum of 1 GeV/c to 2 GeV/c. The production target is made of a platinum rod with the size of 6 mm wide, 3 mm thick and 60 mm long. The secondary particles of K^-, π^- and $\bar{p}$ produced in the direction of 0 degree were bent with the dipole magnet D1 by 23 degree. The beam was focused at the position of the momentum slit by quadrupole magnets Q1 and Q2. Then it passed through an electro-static mass separator (SEP) of 6 m long which had electrodes with 10-cm gap providing electro-statical field of 60KV/cm vertically. The particles were splitted in respect of the mass by SEP, and then vertically focused by quadrupole magnets Q3 and Q4 at the position of the mass slit with a gap of 1mm which discriminated K^-'s from π^-'s and $\bar{p}$'s. The vertical position of the K^- was adjusted by the correction magnet (CM) in order to get the highest yield of K^-'s. Finally, the beam was bent and focused on the SCIFI-target by the dipole magnet D2 and the quadrupole magnets Q6 and Q7.

We used the K^- of 1.66 GeV/c, since it gave maximum yields for the (K^-, K^+) reaction. Typical intensity of K^- was 2×10^4/spill with the primary proton of 2.1×10^{12}/spill. Typical K^-/π^- ratio was 1/4.

2.2 Beam spectrometer

The identification and the tracking of the incident particles were performed with two scintillation counters (T1, T2), a silica aerogel Čerenkov counter (BAC) and 5 sets of multi-wire proportional chambers (BPC1 − 5). These counters were placed upstream of the SCIFI-target as shown in Fig. 2.

The T1 and T2 are made of plastic scintillators (NE pilot-U) of 5 mm thick, 5 cm high, and 10cm and 5 cm wide, respectively. Each of them was viewed by two sets of photo-tubes (HAMAMATSU R2083) from both ends. The T1 and T2 were located 6 m apart from each other. The signal from them were used to get the time-of-flight information of the incident particles with the resolution of 85 psec (r.m.s.).

Blocks of slica aerogel (BAC) were used to eliminate π^-, μ^- and e^- in the incident beam. They had a refractive index of 1.041 which corresponded to the β threshold of 0.961 for the Čerenkov radiation. The blocks had sizes of 8 cm wide, 8 cm high and 3 cm thick and were viewed by a photo-tube (HAMAMATSU R1250). It was sensitive to the Čerenkov light from the incident π^- of 1.66 GeV/c ($\beta=0.997$) but was not sensitive to the incident K^- with the same momentum ($\beta=0.959$). The rejection efficiency for the π^- was more than 99%.

The BPC's were MWPC's having anode wires with 1 mm spacing and carbon-

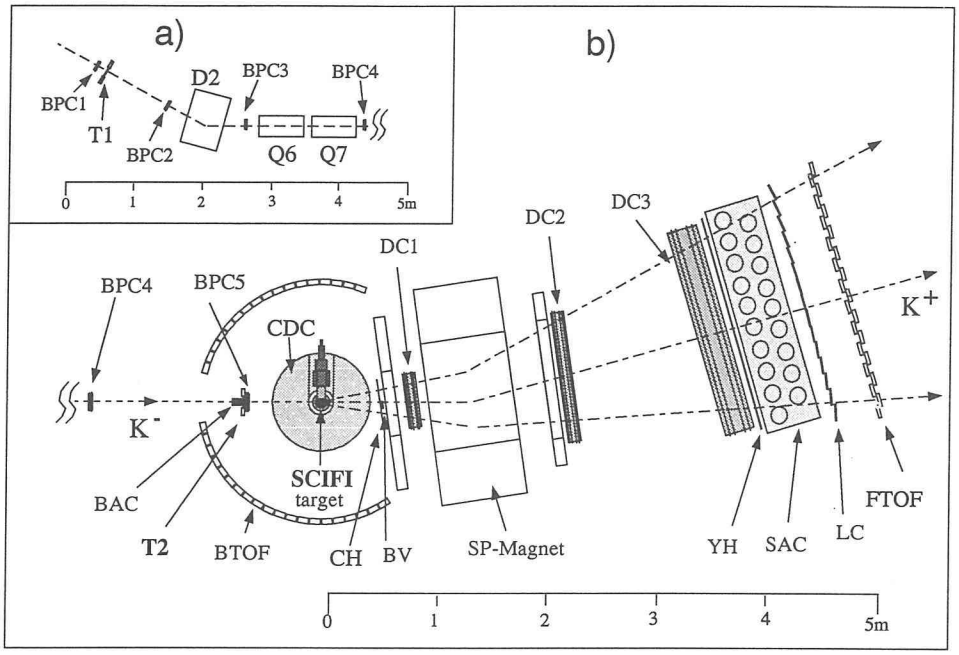

Fig. 2. The top view of the experimental setup. a) The beam spectrometer. b) The K^+-spectrometer. See the text about the description of each component.

coated cathode planes. The "magic gas", mixture of Ar, freon (CF_3Br), C_4H_{10} and methylal with mixing ratio of 73:24:0.5:3 was used for BPC's. The incident particles were tracked with BPC1, BPC2 and BPC3 located upstream of D2, and BPC4 and BPC5 located downstream. The tracks obtained with BPC's were used to determine the momenta of the incident particles and gave the positions in the SCIFI-target.

2.3 K^+-spectrometer

2.3.1 *Spectrometer magnet*

The window-frame-type dipole magnet was located 130 cm downstream of the target, which anayzed the momenta of scattered particles. The pole piece was 80 cm long, 50 cm high and 100 cm wide. The end-guard plates of 8 cm thick were equipped both upstream and downstream of the magnet. The aperture of the downstream end-guard was 100 cm wide and 60 cm high, whereas the upstream one was 50 cm wide and 30 cm high. The direction of the magnet was rotated by 0.15 rad. with respect to the beam direction. The maximum field strength was 1.1 T and $B \cdot dl$ was 1.08 T·m for particles with momentum of 0.8~1.3 GeV/c.

2.3.2 *Drift chambers*

The drift chambers DC1, DC2 and DC3 were located downstream of the SCIFI-target to track the scattered particles. The DC1 was placed at the entrance of the spectrometer magnet. The DC2 was located just downstream of the spectrometer magnet. The DC3 was located 120 cm downstream of the DC2.

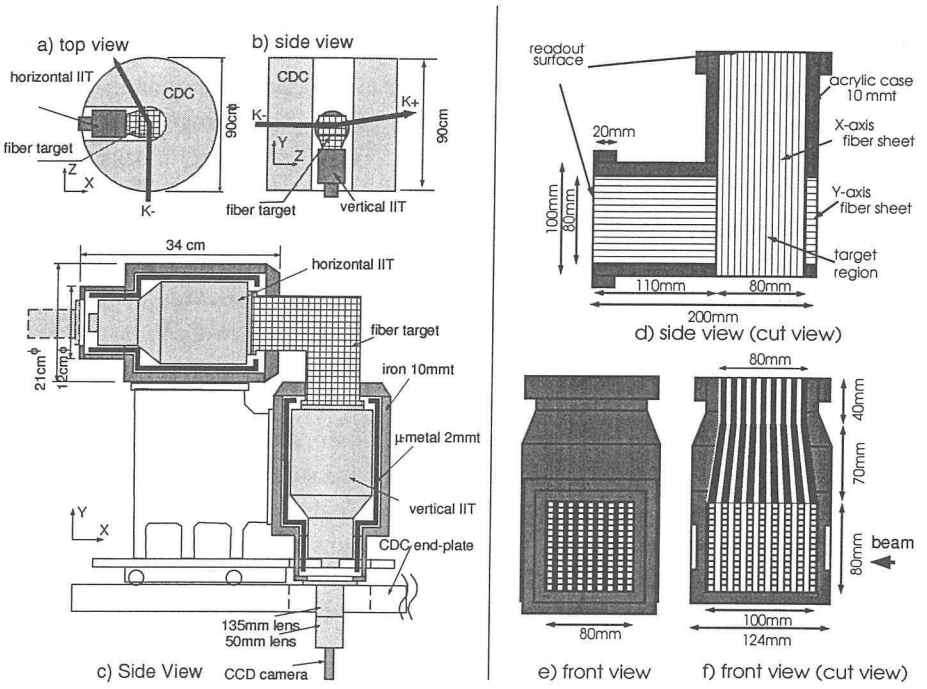

Fig. 3. A schematic view of the setup of CDC and the SCIFI-target; a) the top view and b) the side view. The SCIFI-target was installed inside of CDC. The side view of the SCIFI-target and read-out system are shown in c). d) The side cut view of SCIFI-target, e) the front view and f) the front cut view of the target are shown.

The cylindrical drift chambers (CDC), which surrounded the SCIFI-target as shown in Fig 3, was used to detect reaction products escaped from the SCIFI-target as well as the incident K^-'s and the outgoing K^+'s. The inner radius of the CDC was 16 cm, and the outer radius was 38.4 cm. The height of CDC was 90 cm. The CDC consisted of 6 vertical layers and 2 stereo layers with wires tilted by 5.71° to the vertical direction. The anode wires were made of gold-plated tungsten of 20 μmϕ. The potential and field-shaping wires were made of gold-plated Cu-Be of 100 μmϕ. The typical efficiency was 93% to 96%. The position resolution was 270 μm.

Mixed gas of Ar-ethane (1:1) was used for the drift chambers. The specifications of the DC's are summarized in Table. 2.

Table 2. The specification of the drift chambers.

chamber	DC1	DC2	DC3
plane	XX'YU	XX'YY'	XX'YY'
anode-wire spacing (mm)	10	9	X:56/Y:60
number of read wire	XX':48/Y:32/U:40	XX':128/YY':96	XX':32/YY':16
sensitive area X×Y (cm)	50×35	120×120	180×90
typicall efficiency (%)	99.5	90.3	93.5
position resolution (μm r.m.s.)	XX':220/Y:400/U:200	XX':230/YY':270	XX':310/YY':390

2.3.3 Aerogel Čerenkov counter for spectrometer

The silica aerogel Čerenkov counter (SAC) with sensitive area of 200 cm wide and 100 cm high was located downstream of the DC3. It eliminated the contamination of π^+ 's in the scattered particles. The refractive index of the silica aerogel was 1.041 which corresponded to the β threshold value of 0.961. The silica aerogel blocks of 25 cm$\times$ 25 cm$\times$3 cm were stacked in three layers along the beam direction. The blocks were installed in a diffusion box of which walls were covered with white paper (Milipore). The box was viewed by 38 photo-tubes (HAMAMATSU R1250 and RCA 8854) from the top and bottom. The averaged number of photo-electrons was about 3 for the minimum ionizing particle. The trigger efficiency for K^+ of 1.6 GeV/c was 85%, and the efficiency for π^+ with a momentum above 1 GeV/c was 90%.

2.3.4 Scintillation counters

There were three hodoscopes and one veto counter which were made of plastic scintillators. The specification of the hodoscopes are summarized in Table. 3. The forward TOF hodoscope was used for the "time-of-flight" measurement to obtain the velocity of the scattered particles. The "time-of-flight" (TOF) of scattered particles were measured between the T2 counter and the forward TOF hodoscope (FTOF). The FTOF was located 5 m downstream of the SCIFI-target. The typical resolution was 110 psec (r.m.s). Each counter of FTOF provided the vertical hit position by means of the time difference between the signal from two photo-tubes of both ends. The spatial resolution of 14.8 mm (r.m.s) was obtained.

The hodoscope CH was located just upstream of the spectrometer magnet and used to provide the scattering angles of particles for the first-level trigger as well as the second-level trigger. The hodoscope YH was placed just upstream of SAC to defined the geometrical acceptance of the spectrometer which was 0.09 sr. for the particle with the momentum of 1.1 GeV/c. The non-interacting beam veto counter (BV) was a plastic scintillation counter placed just upstream the spectrometer magnet. It was used to veto non-interacting K^-'s. This counter covered the angular accesptance of $\theta \leq 0.063$ rad. to the beam trajectory.

Table 3. The specification of the hodoscopes.

hodoscope	CH	YH	FTOF
direction	X	Y	X
number of counter	12	6	24
dimension (cm)	$3.5^w \times 17^h \times 0.1^t$	$196^w \times 16^h \times 0.4^t$	$12^w \times 130^h/110^h \times 3^t$
read out	single side	both side	both side

2.4 Trigger logic and data acquisition

The trigger was consist of two levels. The first level trigger was made with information from sevral counters. The coincidence signal of the two beam counters T1 and T2 with the veto-signal from BAC was used to define the incident K^-. The K^- which didn't interact in the target was rejected with the veto signal from the BV counter. The outgoing particles with positive charge were selected by the matrix-

coincidence-logic (charge trigger) which identified the charge with the bending angle deduced from the combination of the hit positions of CH and FTOF. Then "K^+" was defined as the coincidence signal of CH and FTOF with the veto signal from SAC for π^+'s rejection. In addition, a signal from YH was required in order to reject neutral particles. The first-level trigger was applied to the second stages of the IIT's, and it initiated the DAQ sequence for the spectrometer system. Standard CAMAC and TKO system were used for the DAQ. The digitized data were stored in CAMAC memory modules, then read out by a computer every at the end of spill.

The events selected by the first-level trigger contained (K^-, p) reactions as the major backgrounds. Pure K^+'s were selected as the produced particles in the second-level trigger using information of the mass which was obtained by the time-of-flight between FTOF and T2 as well as hit positions at CH and FTOF.

The trigger rate of protons were reduced by factor of 10 by means of this procedure. The efficiency was greater than 90% for the K^+ with the momentum larger than 700 MeV/c. A typical trigger rate was 55 Hz for the first-level trigger and 10 Hz for the second level trigger with the K^-'s of 1×10^4/sec.

The second-level trigger was applied to the third stage of the IIT's, and it initiated the DAQ sequence of the SCIFI-data, which were read out continuously by VME computers. The correspondence between the spectrometer data and the SCIFI-data was made by the sequential event number, which were fed into both of the DAQ systems.

3 The SCIFI-target system and the method of data analysis

3.1 Structure of SCIFI-target

3.1.1 Scintillating fiber block

The SCIFI-target consisted of about 30,000 plastic scintillating fibers of 20cm long. The scintillating fiber (KURARY SF-81) had a square cross section with the dimension of 500 μm $\times$ 500 μm. The core size was 480 μm square, and the clad thickness was 10 μm. The core material was made from polystyrene of which refractive index was 1.59 and density was 1.06 g/cm^3. The cladding material was made from poly-methylmethacrylate (PMMA) of which refractive index was 1.49 and density was 1.18 g/cm^3. The spectrum of the transmitted light had a peak at 437 nm.

The schematic view of the scintillating fiber block is shown in Fig. 3-d), e) and f). Sheets which consisted of 160 fibers were stacked alternately in the X (horizontal) and the Y (vertical) directions to provide three-dimensional views of the tracks of particle. The number of stacked fiber-sheets was 92 for each direction. The sheets were bonded with black acrylic glue of 50 μm thick, which also worked as extra mural absorber (EMA) in order to eliminate crosstalks of photons over the sheets. Overall effective areas were 8 cm $\times$ 10 cm in both X-Z and Y-Z planes. The sizes of the images were reduced to 8 cm $\times$ 7.8 cm on the readout surfaces where the sheets were stacked with spacers of 350 μm in thickness alternately. The stack of sheets was mounted in an acrylic case of 1 cm thick. The other ends of fibers were equipped with LED light sources through holes on aluminum plates for providing the position references.

3.1.2 Image intensifier tube

The SCIFI-target was viewed by two sets of the image intensifier tube (IIT), which amplified the photon images of tracks and were gated with external triggers in order to select events of interest. The IIT's (Delft PP0040) were assemblies of 3 stages of image intensifiers.

The first stage was of an electrostatic type operated with DC voltage of 20 KV. The diameter of the input window was 80 mm ϕ, and that of the output window was 18 mm ϕ. Both input and output windows were made of glass fibers with diameter of 10 μm. The photo-cathode of the input window was equipped with S20. The photons from the scintillating fiber were converted to photo-electrons, and the image was demagnified by factor 5 with an electrostatic lens. Photons were produced by means of the bombardment of photo-electrons on P24 phosphor, of which decay time was 2.4 μsec, at the front of the output window made of optical fiber. Average production rate of photon per electron was 8 in the case that the voltage applied between the cathode and the anode was 20 KV.

In the second stage a micro-channel-plate (MCP) was used to multiply photo-electrons. Owing to the MCP, it had high photon gain with rather low voltage (10^3 at 750 V) and was easily triggered by changing the applied voltage between the cathode and the MCP. The MCP was gated by the first-level trigger as described later. The input and output windows had the diameters of 18 mm. The photo-cathode was made of S20. The output window was equipped with P20 phosphor of which decay time was approximately 50 μsec. The third stage was the same device as the second stage, whereas the MCP was gated with the second level trigger.

The IIT's were put in the magnetic shield to eliminate the fringing field of the spectrometer magnet, since the effect to the trajectories of photo-electrons caused distortion of image. The shield consisted of two layers, the outer layer made of iron (SS-41) of 25 mm thick, and the inner layer made of μ-metal (TMC-V) of 2 mm thick. The field along the tube direction in the shield was about 3 gauss for the vertical IIT and about 1.5 gauss for the horizontal IIT whereas 30 gauss was measuered outside of the sheild.

Since photon emission from the phosphor continued during the decay time of phosphorescence, the time resolution of the IIT was determined by the decay time, and the phosphor played a role of "optical delay" of the image. It enabled us to select images of interest using trigger pulses from the counter system. Considering the beam intensity (10^5/sec) of the present experiment, we used the IIT's of electro-static type with the phosphor whose decay time was 2.4 μsec in order to prevent the exposure for more than two events in one picture. The decision time of the first-level trigger was 300 ns, thus the image had to be kept for the period. The first-level trigger was used to open the gate of the second stage, which kept the image for the phosphor decay time of 50 μsec. The second-level trigger was applied to the third stage, of which output was detected with a CCD camera.

3.1.3 CCD video camera and image digitizer

The photon images amplified with each IIT were viewed by a charge-coupled-device (CCD) camera through the optical lens systems. The lens system consisted of

compound lenses of 135 mm and 50 mm coupled in tandem, where the lens of 135 mm attached reversely. The lens system demagnified the images from 16 mm to 6.6 mm for matching the image size to CCD-chip size. The CCD camera (SONY XC-77) contained a CCD-chip having 768×493 pixels of 11.0 μm $\times$ 13.0 μm. Since every two pixels were packed into one in the digitization, the effective pixel size was 22.0 μm $\times$ 13.0 μm. The size of the CCD-chip was 8.8 mm $\times$ 6.6 mm.

The NTSC video signals from the CCD cameras were digitized with the image digitizer. The digitizer provided a common clock to synchronize the CCD cameras, and generated two-dimensional coordinates of each CCD pixel. The CCG module initiated a sequence of digitization when the second-level trigger occurred. A "CCD busy" signal was asserted during the read-out sequence in order to prohibit image overlap due to another track. The deadtime due to the CCD read-out was effectively 25 msec.

The pulse heights of the video signals were digitized into 7-bit data of brightness for each pixel. Then the pixel data, which consisted of 10-bits for the X-coordinate, 9-bits for the Y-coordinates, 7-bits for the brightness and 6-bits for the serial event number, were stored in FIFO memory when the brightness was above the preset threshold.

A typical number of pixels for one event was about 2,000, while the FI/FO buffer memory could storage the data of about 4,000 pixels. The data in each FIFO module were continuously read out by a standard VME FI/FO module, whenever the FI/FO buffer memory was not empty.

3.2 Basic performance of the SCIFI-data

Figure 4-a) shows typical pictures of a π^- of 1.6 GeV/c, a minimum ionizing particle (MIP) in the SCIFI-target. The left picture shows the X-Z projection obtained by the vertical IIT and the right picture shows the Y-Z projection obtained by the horizontal IIT. The gray-scale of small rectangles in Fig. 4-b) represents the brightness of the CCD pixels after pedestal subtraction. The fiducial areas defined by the size of the IIT and the CCD are shown as the areas surrounded with the lines in the pictures.

Most of the clusters of the rectangles shown in Fig 4-b) correspond to the image of one photon. We have applied the method of two-dimensional clutering to the CCD pixels with the weight of the brightness. The cluster spreads over 3×3 pixels typically with sigma of 180 ± 40 μm as shown in Fig. 5-a). The track has been identified as a sequence of clusters. The density of the cluster for a MIP track has been found to be 0.55/mm. The position of a cluster has been obtained as the center-of-gravity of the brightness of pixels, and the position resolution deduced from the residual distribution of the straight line fit on the clusters is 290 μm as shown in Fig.5-b).

This resolution, σ_c, has been evaluated as;

$$\sigma_c \sim \sqrt{\sigma_{fiber}^2 + \sigma_{CCD}^2 + \sigma_{IIT}^2 + \sigma_{sys}^2} \sim 270\mu\text{m}, \tag{4}$$

where $\sigma_{sys}^2 \sim \sigma_{align}^2 + \sigma_{dist}^2$.

The σ_{fiber} has been estimated to be 500 μm/$\sqrt{12}$ from the size of scintillating

fiber. The σ_{CCD} is about 90 μm which has been obtained from the CCD pixel size, about $\sim$22 μm and the demagnification factor of IIT, about 13. The σ_{IIT} has been measured to be about 30 μm. We have estimated $\sqrt{\sigma_{align}^2 + \sigma_{dist}^2}$ to be 200 μm by a calibration using a reference pictures. The result is consistent with the measured value as shown in Fig. 5-b).

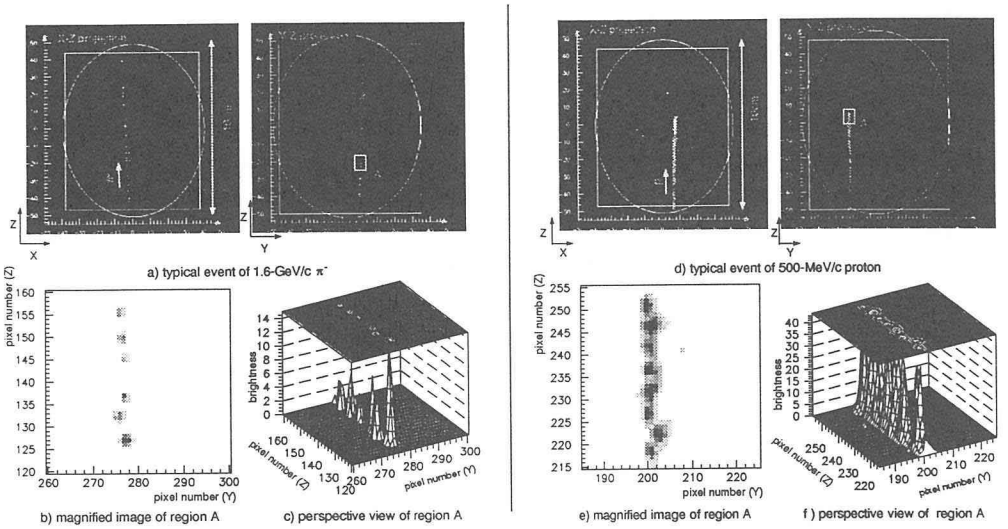

Fig. 4. Typical picture of a minimum ionizing particle. A straight track of 1.6-GeV/c π^- is shown. a) Display of the tarck in the X-Z and Y-Z projections. b) The magnified view of the track in the region A of the Y-Z projection. Here, the axes show the pixel coordinates. Each rectangle corresponds to a pixel where the brightness is presented in gray-scale. c) The perspective view of the plot in b). The pixel brightnesses are shown as the heights. Similar histgrams for a track of a 500-MeV/c proton stopped in the SCIFI-target are shown in d), e) and f).

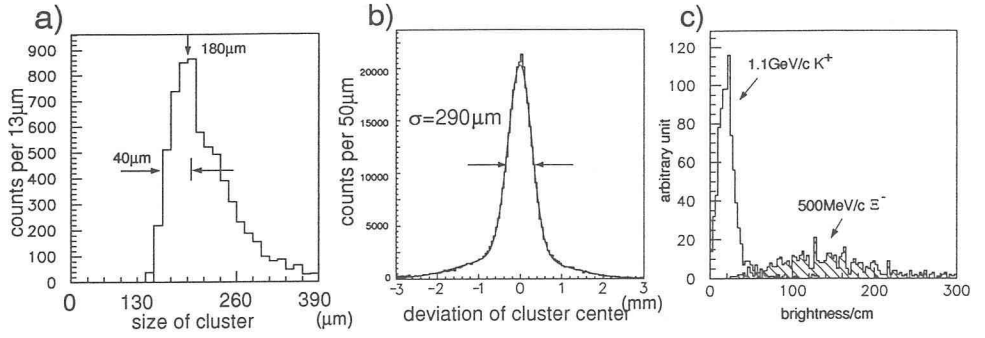

Fig. 5. The distribution of the size of one photon cluster in r.m.s. b) The residual distribution of the straight line fit on the cluster positions in MIP tracks. A fit with two Gaussian distribution reproduces the distribution. c) The distribution of brightness of the tracks of MIP's and of low energy particles.

An example of image of a 500-MeV/c proton which stopped in the SCIFI-target is shown in Fig. 4-e). In contrast to the tracks of MIP's, photon clusters stick together since the ionization of such a particle is more than four times as large as that of the tarck of MIP. We have observed the difference between the tracks of low energy particles and those of MIP's by means of the comparison of the brightness of the clusters along the tracks. Figure 5-c) shows the distribution of density of brightness along tracks of MIP's and that along typical Ξ^- tracks ($\beta \sim 0.4$) produced by the (K^-, K^+) reaction. The figure shows the clear difference between them. In order to treat tracks of MIP's and of low-energy praticles with the same algorism, we have generally use of the straight-line fit on the pixels data weighted by the brightness. The angular resolution for the tracks of MIP's has been evaluated by means of the comparison with the external tracks obtained with the K^+-spectrometer of which angular resolution is less than 3 mrad for MIP's. The angular resolution against the track has been obtained as $\sigma_\theta \sim$ 500/L mrad., where the L is the track length in mm. The contribution of multiple scattering for the angular resolution, which is written as $0.41 \cdot \sqrt{L}$ mrad., is negligibly small for the tracks of MIP's. It is, however, considerably large for the tracks of low energy baryons. For example, the effect of multiple scattering of the 500-MeV/c proton track is given as $2.9 \cdot \sqrt{L}$ mrad.

3.3 Analysis of the SCIFI-data

We describe the method of analysis of the SCIFI-data. First of all, we describe the scanning procedure to find a track in a picture. Then, the methods to obtain three-dimensional track information is presented. Finally we demonstrate the performance of the kinematical reconstruction.

3.3.1 Scanning of events

A typical Ξ^- decay event is shown in Fig. 6. First of all, K^- and K^+ tracks have been recognized using the external position information given by the counter system in the beam line and the K^+-spectrometer. The accuracy of the prediction for the K^+ has been 500 μm for the picture on the X-Z projection and 800 μm for the Y-Z projection. The accuracy for the prediction of the beam position has been about 1mm for both projections. Accidental overlapping of incident tracks have been separated by means of those predictions.

The (K^-, K^+) reaction point has been identified as the cross point of the K^- and K^+ tracks. When the emission of one or more charged particles are observed, the (K^-, K^+) reaction point has been apparently identified as a vertex of multi prongs.

The Ξ^-'s and Σ^-'s have been identified by observing the "kink" topology due to weak-decays such as $\Xi^- \rightarrow \Lambda \pi^-$ and $\Sigma^- \rightarrow n \pi^-$. These weak-decays have been identified also with the sudden change of the brightness, since the ionization of π^-, a decay product, is 1/4 of that of slow hyperons. Weak-decays of Λ's have been identified by "Vee"-like topology formed with the decay products, proton and π^-.

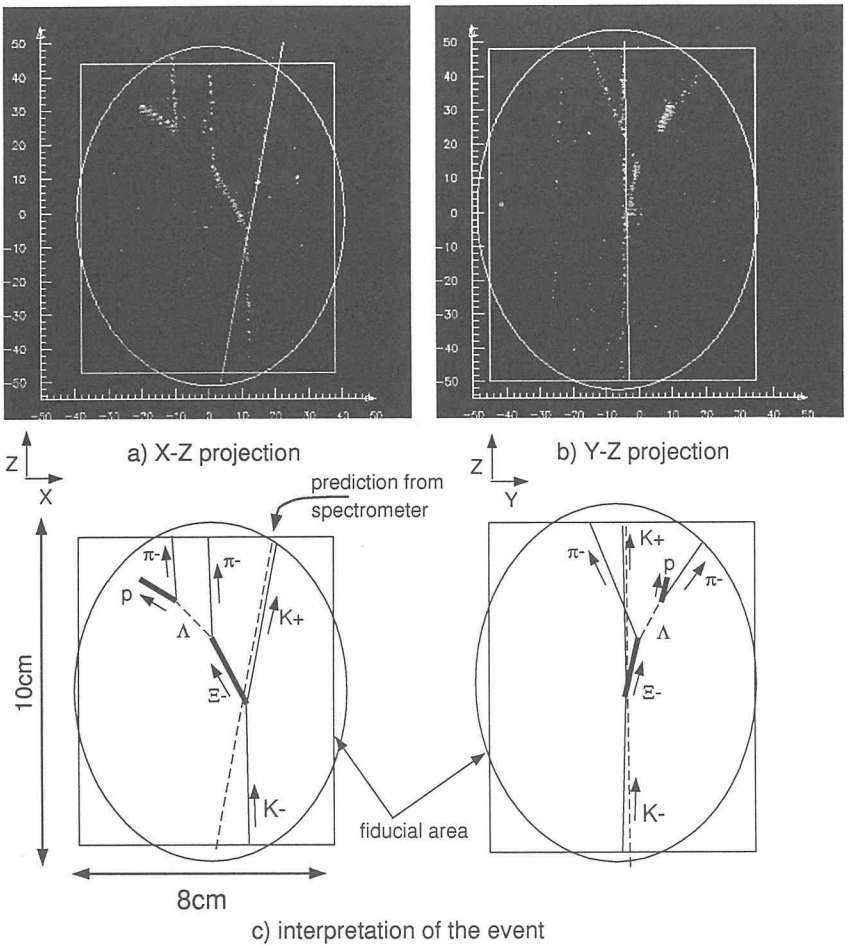

Fig. 6. The display of a typical Ξ^- decay. The weak-decay sequences of $\Xi^- \rightarrow \Lambda + \pi^-$ and $\Lambda \rightarrow p + \pi^-$ are clearly identified. a) The X-Z projection obtained with the vertical IIT. b) The Y-Z projection obtained with the horizontal IIT. The track prediction with the K^+-spectrometer is also shown as lines on both pictures which have good agreement with the images of the track of K^+'s. c) Interpretations of the tracks in a) and b).

Since the tracks on the X-Z and the Y-Z projections have the "same" Z-position, the correspondence between the tracks on the two projections has been done by referring the Z-position of stop or kink points. The tracks of escaped particles, however, may have a stereo ambiguity similar to that of multi-wire chambers. Such an ambiguity can be solved using the external information of the internal kinematical constraint, for example, on the coplanarity.

3.3.2 *Three-dimensional event reconstruction*

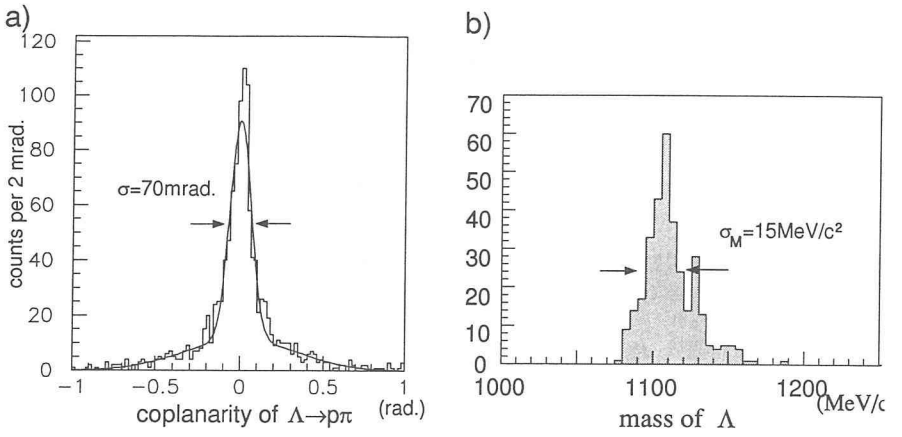

Fig. 7. a) The coplanarities of $\Lambda \rightarrow p\pi^-$ decays. The coplanarity is defined as the angle between the direction of the mother particle and the decay plane. b) The distribution of the reconstructed mass of Λ from Ξ^- decay.

Positions of (K^-, K^+) interactions and decay positions of hyperons such as the Ξ^- and Λ have been measured on an event-display screen. Those positions have been examined by means of the method of the center-of-gravity of the brightness inside the square of 2 mm around the measured position. For the track identification a corridor has been defined along the track, and the pixels in the corridor have been used for the straight-line fit to obtain a two-dimensional track. Finally the tracks in both projections have been combined to obtain a three-dimensional track. The vertex position has been defined as the closest position of the two tracks. The coplanarities of the tracks of the particles in $\Lambda \rightarrow p\pi^-$ decay are shown in Fig. 7-a), which show typical performance of the three-dimensional reconstruction in the SCIFI-target.

3.3.3 *Kinematical reconstruction by means of the range measurement*

The ranges of the particles have been obtained by the position measurement described in the previous section. The kinetic energy can be determined by the range in the SCIFI-target with the Bethe-Bloch formula. We have used the following empirical formula instead of the Bethe-Bloch formula for the sake of simplicity;

Table 4. The coefficients a and b for various particles which are used for the calculation of the kinetic energy from the range in the SCIFI-target. The parameters are given for the range R in cm and the kinetic energy T in MeV (see the text).

	π^-	proton	Σ^-	Ξ^-
a	14.1	32.5	36.3	38.0
b	0.5653	0.5553	0.5535	0.5521

$$T = aR^b, \tag{5}$$

where T is the kinetic energy of the particle, a and b are the constants given in Table 4 and R is the range in the SCIFI-target of the particle. The accuracy for the range measurement has been 1 mm, which corresponds to the energy resolution of 10% for stopped protons of 1 cm long. The calibration has been done with stopped protons with the kinetic energy of 40 MeV at INS SF-cyclotron [33].

If one of the charged particles from two-body decays stops in the SCIFI-target, the mass M_0 and momentum p_0 of the mother particle can be calculated as follows. Using the measured range R and the decay angles θ_1 and θ_2 the momentum of the mother particle, p_0, is determined from the momenta of decay products p1 and p_2 as

$$p_0 = p_1 \cos\theta_1 + p_2 \cos\theta_2,\ p_1 = \sqrt{(a \cdot R^b + M_1)^2 - M_1^2},\ p_2 = p_1 \frac{\sin\theta^1}{\sin\theta_2}. \tag{6}$$

Here M_1 is the rest mass of proton. Then the mass M_0 can be obtained as

$$M_0 = \sqrt{E_0^2 - p_0^2},\ E_0 = \sqrt{p_1^2 + M_1^2} + \sqrt{p_2^2 + M_2^2}. \tag{7}$$

Here we need to assume the mass of the decay products M_1, and M_2. The reconstructed mass distribution of Λ are presented in Fig. 7-b), in which the mass resolution is shown to be 15 MeV/c^2.

3.3.4 Detection efficiencies for scanning

Detection of single tracks: A cluster with 3 photons or more has been required for the identification of the track. Since a track of MIP produces a cluster with 0.55 photon per mm in average, the track of 15 mm long has about 8 photons, which gives the detection efficiency of about 99%. If a particle doesn't pass through two layers of the scintillating-fiber-sheets, the track appears only in the X-Z or the Y-Z picture since the fiber-sheets are stacked alternately for both directions. A track must be longer than 1.5 mm (more than 3 layers) along the beam axis for three-dimensional reconstruction.

Detection efficiency for Ξ^-: The Ξ^- and Λ are identified by observing their weak-decay topologies that show "kink-track" or "Vee-track" in pictures. The detection efficiency for Ξ^-'s is low in the case that the decay position of Ξ^- is close to the vertex point of the (K^-, K^+) reaction. Such a low efficiency is due to the minimum visible distance between the vertex position and the decay position in the SCIFI-target. It is shown in the decay length distribution of Ξ^- in Fig. 8-a). The detection efficiency, η_Ξ, as a function of the decay length, R_Ξ, was deduced by comparing the measured decay length distribution to that of the Monte Carlo simulation. The efficiency is consistent with unity if the decay length is longer than 5mm as shown in Fig 8-b). We neglect the dependence of the efficiency on the flight length of π^-, R_π, since the track of π^- produced in the Ξ^- decay has sufficiently long flight length in the SCIFI-target.

The detection efficiency for Λ: The similar effects are also observed in the detection of Λ's by means of the search for "Vee-track". In this case, the efficiency, η_Λ, depends on the Λ decay length, R_Λ, and the flight-length of the shortest decay products, R_p.

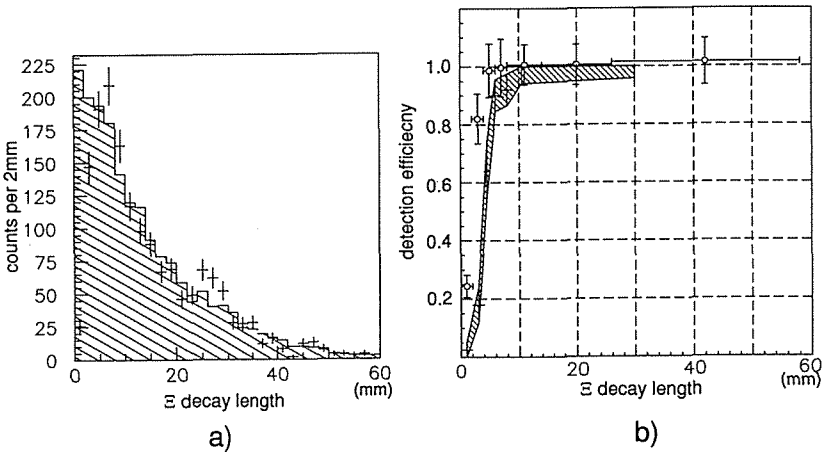

Fig. 8. a) The decay length distribution of Ξ^-'s which are associated with charged decays of Λ's is shown with the crosses. The hatched histogram shows the result of a calculation by a Monte Carlo simulation. The normalization has been done in the region where the decay length is 10 mm to 30 mm. b) The detection effciencies for Ξ^-'s as a function of the decay length are shown as the open circles. The error bar corresponds to 1 σ of the statistical error. Also are shown the detection efficiency deduced from the simulated pictures. The width of the hatched area corresponds to 1 σ of the statistical error.

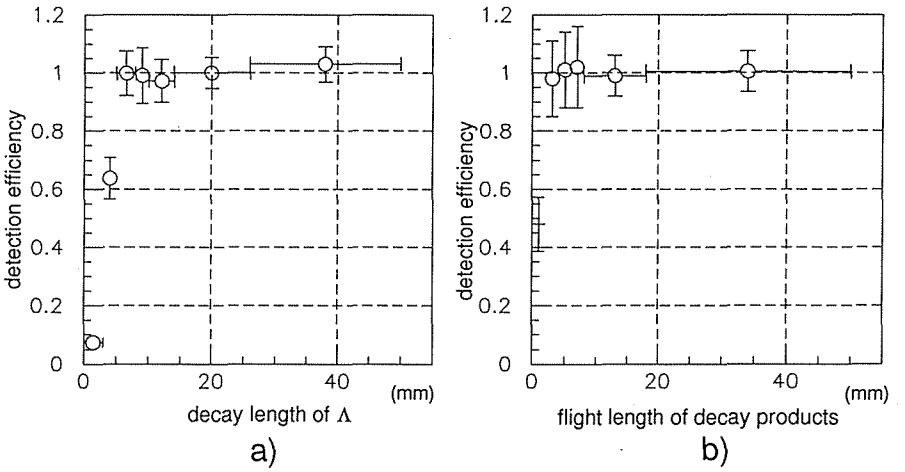

Fig. 9. a) The detection efficiency for Λ as a function of its decay length R_Λ where R_p is longer than 5mm. b) The detection efficiency for Λ as a function of the flight length shortest track of its decay products R_p, where R_Λ is longer than 5 mm.

The decay length distribution of Λ and the flight length distribution of the shortest decay products in the Λ decay are obtained from the Ξ^- decay events. We have evaluated the detection efficiency of Λ by comparing them to the expected

distributions derived from a Monte Carlo simulation. Figure 9 shows the efficiencies as a function of the decay length of Λ, $\eta_\Lambda(R_\Lambda)$, and that as a function of the length of the shortest decay products, $\eta'_\Lambda(R_p)$. The efficiencies, $\eta_\Xi(R_\Xi)$ and $\eta_\Lambda(R_\Lambda)$ are in good agreement each other, while $\eta'_\Lambda(R_p)$ shows higher values in the region of $R_p \leq 5$ mm.

Examination by the simulated pictures: We have exmained $\eta_\Xi(R_\Xi)$ and $\eta_\Lambda(R_\Lambda, R_p)$ by scanning the simulated pictures generated by the GEANT program. The pictures of quasi-free Ξ^- productions in $(CH)_n$ with the decay sequences have been reconstructed by the same method as the analysis of the experimental data. The obtained efficiency curve for finding a Ξ^- as a function of the decay length agrees with that of the experimental data a shown in Fig. 8-b). In the region $R_\Xi \geq 5$ mm, 147 events have been found to be detected among 155 generated samples. It corresponds to the efficiency of 95%. The $\eta_\Lambda(R_\Lambda, R_p)$ also has been examined by scanning the same pictures. In the region of $R_\Lambda \geq 5$ mm and $R_p \geq 5$ mm total 44 events among 46 generated samples are detected. It corresponds to the efficiency of 95%. Two events have not been found due to the accidental overlapping of tracks described below.

Inefficiency from other sources: We discuss the origins of inefficiency which are not attributed to the minimum visible distance between two tracks. Several cases are considered.

One of the sources is an accidental overlap of tracks at a vertex point. Such kind of inefficiency occurs when a K^+ track or a tracks of beam particle overlap accidentally at the vertex point of a "Vee-track" in both of the X-Z and Y-Z pictures. The effect becomes negligible if the distance between the vertex point and the track of the particles is longer than 1 mm in either picture. The inefficiency due to the overlapping has been estimated to be about 2% in the case of Ξ^- decays.

The inefficiency comes also from the uncertainty of determination of the angle between two decay products. The minimum detectable angle of a "kink-track" has been estimated from the angular resolution of the SCIFI-target, which is about 50 mrad. for a track of 1cm long. Although the inefficiency owing to such an origin is negligible in the case of Ξ^- decay, but the effects are strongly correlated with the event kinematics. Detailed evaluation of the detection efficiency for the $H \rightarrow \Sigma^- p$ search is discussed in Section 4.

4 Analysis of the possible candidates for the H particle

4.1 Pre-selection by (K^-, K^+) tagging

4.1.1 Analysis of K^-

We have collected 5×10^6 triggers in the SCIFI-target. The background events due to other reaction included in the (K^-, K^+) reactions have been eliminated in the off-line analysis in order to obtain true (K^-, K^+) reactions.

The K^-'s have been selected using the information of time-of-flight between T1 and T2 in the off-line analysis. The TDC data of T1 and T2 have been corrected with the pulse hight information obtained with the ADC data. The resolution of time-of-

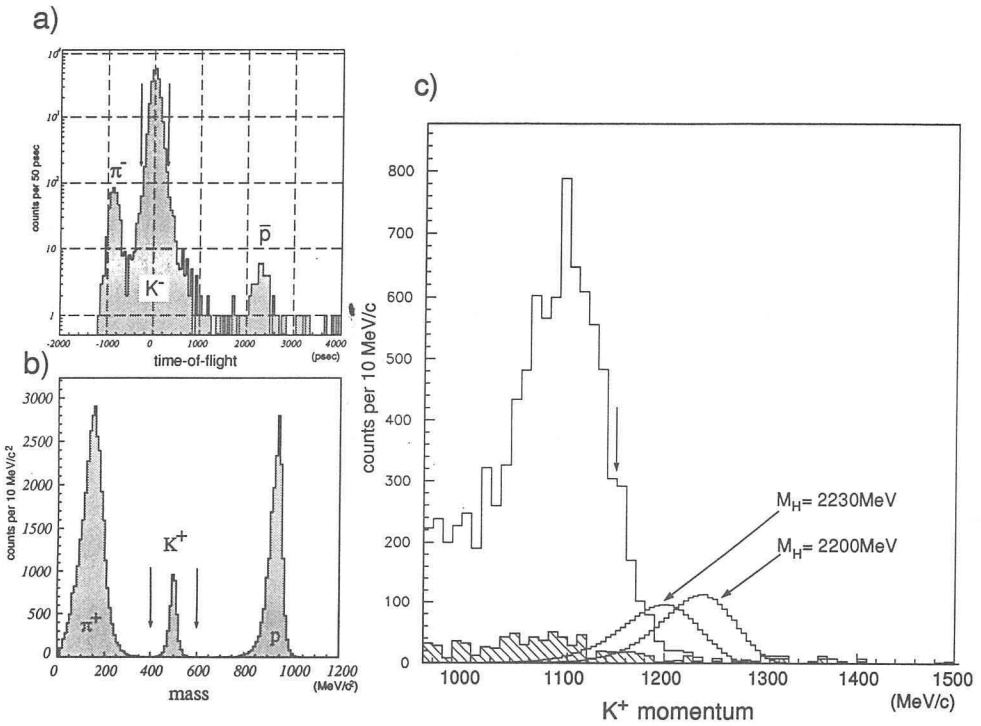

Fig. 10. a) The TOF spectrum of the incident particles. The arrows show cut values to obtain K^-'s. b) The mass spectrum of the scattered particles. The particles in the region between two arrows have been selected as the K^+'s. c) The momentum spectrum of K^+. The plain histogram shows the data before the deduction by SCIFI-data. The hatched histogram shows the background events rejected by scanning SCIFI-data. Also shown are the peaks corresponding to the direct H production for M_H= 2200 MeV/c^2 and M_H=2230 MeV/c^2 in the process,$K^- + (pp) \rightarrow K^+ + H$ expected from a Monte Carlo simulation. The arrow shows the K^+-momentum cut to analyze the data of direct H production.

flight was 85 psec. The obtained histogram of the time difference between T1 and T2 is shown in Fig.10-a). To reject the contamination with π^- and $\bar{p}$, we have used K^-'s of which deviation from the center of the time-of-flight spectrum was within $\pm$ 300psec. The tracks of the K^-'s have been obtained from the hit positions on BPC3-5 and CDC using the beam transportation matrix, They have been useful for the position prediction of K^- in the SCIFI-target. The reconstruction efficiency has been 80%.

4.1.2 Analysis of K^+

The tracks of scattered particles have been obtained from the hit positions on CDC, DC1, DC2, DC3 and FTOF. The FTOF has provided the vertical position by using the time difference between the signal from the photo-tube on both the top and the bottom of the counter. The spatial resolution is 14.8 mm in vertical direction. We required the hits all on the vertical and horizontal planes of DC1, DC2, DC3 and at

least 4 hits on CDC in the region of the acceptance of the K^+ -spectrometer. We have rejected the tracks of which positions predicted by FTOF is different from the positions of the tracks bv more than 7 cm in horizontal or than 3 cm in vertical. The background events due to K^- decays have been rejected with this cut. The tracking efficiency is about 80% in total.

The velocity of the particle has been determined by the time-of-flight measurement between T2 and FTOF after pulse-hight correction of TDC data. The resolution of time-of-flight is 110 psec. The mass of the scattered particle has been obtained from the momentum and the velocity. The obtained mass distribution is shown in Fig.10-b). The particles in the mass region of 400 MeV/c^2 to 600 MeV/c^2 of the spectrum has been selected as the K^+'s. The mass resolution for the K^+ is 18.5 MeV/c^2. The obtained momentum spectrum for K^+ is shown in Fig.10-c). The momentum resolution has been obtained to be 0.5% at 1.1 GeV/c.

The total number of the (K^-,K^+) reactions tagged by the spectrometer is about 10,000. The number of contamination misidentified as the K^+ deduced from the tail of mass spectrum is less than 1% of the total number of the K^+. The backgrounds are from (K^-, π^+) reactions. Another background is due to the K^0 production, which are eliminated by analyzing the SCIFI-data as explained in Section 4.2.

4.2 Scanning of quasi-free (K^-,K^+) reaction

The pictures of (K^-,K^+) reactions tagged by the spectrometer have been scanned by human eyes and have been categorized to the (K^-,K^+) reactions into several cases according to the event topologies[33]. The results of the classification are shown in Table 5. We Have required that the (K^-,K^+) reaction point has been observed in the fiducial area. We have rejected the background events due to the neutral kaon productions;

$$K^- + p \rightarrow \overline{K^0} + n, \quad \overline{K^0} \rightarrow K^0, \quad \text{then} \quad K^0 + p \rightarrow K^+ + n, \tag{8}$$

and

$$K^- + p \rightarrow \overline{K^0} + n, \quad , \quad \text{then} \quad \overline{K^0} \rightarrow \pi^+ + \pi^- \tag{9}$$

Table 5. The numbers of (K^-,K^+) events and background events deduced by scanning the pictures. Here "prediction mismatched" means the events of which positions of K^+ tracks mismatches with the predicted tracks from K^+ -spectrometer.

	$P_{K^+} \geq 950$ MeV/c	$P_{K^+} \geq 1150$ MeV/c
(K^-,K^+) in fiducial	8294	697
(K^-,K^+) out of fiducial	1537	149
neutral kaon	172	57
prediction mismatched	359	44
double scattering	47	8

In the latter case,the π^+ has been miss-identified as the K^+. These events have been rejected by observing the disconnection of the K^- track and the K^+ track which corresponds to the neutral kaons. We have rejected the events of which K^- or the K^+ were scattered additionally in the picture. We have rejected also the events of which the positions of the K^+ tracks mismatch with the predicted position given by the information from the spectrometers.

The number of (K^-, K^+) reactions after these selections is 8,294. We have studied the pictures more carefully in the region where K^+ momenta are greater than 1150MeV/c in order to search for the H dibaryon which decays into Σ^- and proton.

4.3 Search for the H decay in $P_{K+} \geq 1150$ MeV/c

4.3.1 Expected signal of the H : decay topology

In this section we discuss the kinematics of production and decay of H into $\Sigma^- p$. We have searched for the H produced in a carbon nucleus directly through the process;

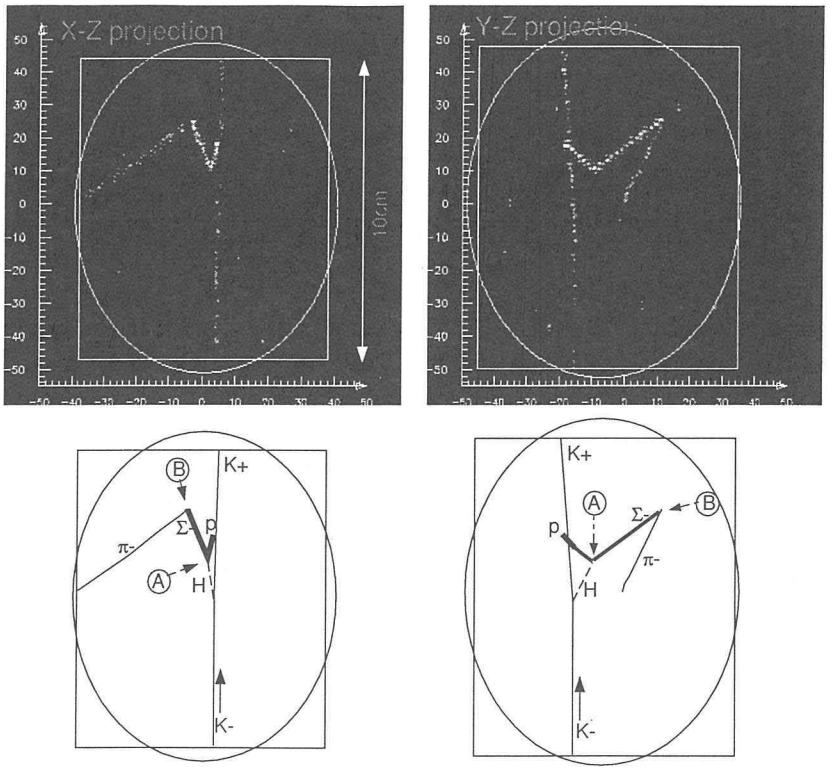

Fig. 11. A typical track image of $H \rightarrow \Sigma^- p$ generated by the GEANT simulation. The production of H via a reaction $K^- + (pp) \rightarrow K^+ + H$ and sequential weak decays, $H \rightarrow \Sigma^- + p$,then $\Sigma^- \rightarrow n\pi^-$ are shown. Such a track image is named as "kinked Vee-track" which is expected to be detected in the SCIFI-target(see the text).

$$K^- + (pp) \rightarrow H + K^+, \tag{10}$$

where (pp) is a proton-pair in a carbon nucleus.

The momentum distribution of K^+'s for the H mass of interest has been calculated by a Monte Carlo simulation assuming the process above. The results are shown in Fig.10-c). The momentum of K^+ decreases with the increase of the H mass. The lower limit of K^+ is about 1100 MeV/c for $M_H = 2230$ MeV/c^2. We have put an emphasis on the heavy H search (2200 MeV/$c^2 \leq M_H \leq$ 2230 MeV/c^2). We have analyzed the events in which K^+'s have momenta higher than 1150 MeV/c. This cut gives 90% efficiency for the analysis.

Under these constraints,the reactions;

$$K^- + (pp) \rightarrow H + K^+ + \pi^0, \quad \text{and} \tag{11}$$
$$K^- + (pn) \rightarrow H + K^+ + \pi^- \tag{12}$$

are not allowed kinematically. Therefore,no charged particles should be observed at the (K^-, K^+) vertex point except short ones (less than a few cm) which are possibly low-energy protons evaporated from the residual nucleus.

A signature of the H is the sequential weak decay chain;

$$H \rightarrow \Sigma^- + p, \quad \text{then} \quad \Sigma^- \rightarrow \pi^- + n. \tag{13}$$

Fig.11 shows at typical event of the H decay generated by a Monte Carlo simulation. About 70% of the H with the lifetime of 3×10^{-10} is expected to decay in the SCIFI-target.

The charged decay products, the Σ^- and proton, show a topology of a "Vee-track" which is similar to that of $\Lambda \rightarrow \pi^- p$ decay. Since the ionization of Σ^- and proton are more than 4 times as large as these of minimum ionizing particles, a significant difference "brightness" of the tracks from minimum ionizing tracks can be observed. About 50% of the protons stops in the SCIF-target and the rests escape from target. The mean decay length of Σ^- is about 10 mm. About 60% of Σ^-'s is expected to decay into π^-n with the 100% branching ratio in the SCIFI-target,and about 10% is expected to stop and interact with material in the SCIFI-target. The rests are expected to escape from the target. A momentum of the π^- from the Σ^- decay is around 200 MeV/c. Although about 99% of π^- have momenta sufficient to escape from the SCIFI-target, the reaction cross section of π^- is large at this momentum region (about 360 mb for carbon) because of the Δ resonance. Thus some of the π^-'s interact with a nucleus in the target. Taking this effect into account, we have estimated that the probability of escape of π^- from the target is about 90%. It produces a minimum ionizing track in the picture. Thus the decay chain of the H is observed in the picture as a "kinked Vee-track" as shown in Fig.11, which we search for as the signature of H.

4.3.2 Requirements to search for "kinked Vee-track"

Considering the conditions discussed above, we have set the following requirements for the "kinked Vee-track" as a $H \rightarrow \Sigma^- p$ candidate.

Requirement A: The two kink points, the decay point of $H \rightarrow \Sigma^- p$ (A in Fig.11) and

the decay point of $\Sigma^- \rightarrow n\pi^-$ (B in Fig.11), are observed in the fiducial area of the picture.

Requirement B: The π^- from the Σ^- decay has a flight length longer than 15 mm before it escapes from the fiducial area of picture.

The Requirments A and B is the definition of the event topology of H decay. As discussed in the case of the Ξ^- decay in Section 3, the H whose decay point is close to the production point is difficult to be detected by scanning. The same difficulty occurs also for the decay of Σ^-. To evaluate detection efficiencies of these events, we have considered a "kinked Vee-track" as a combination of a "Vee-track" and a "kink-track". Then the detection efficiency of the "kinked Vee-track", η_{KV}, is evaluated as a simple multiplication of the detection efficiency for Ξ^-, η_{Ξ}, and that for Λ, η_{Λ}, as;

$$\eta_{KV} \sim \eta_{\Lambda}(R_H, R_p) \times \eta_{\Xi}(R_\Sigma) \times \eta_o \tag{14}$$

The η_{KV} is the detection efficiency of the H in the scanning of the "kinked Vee-track" in the pictures. Here we used R_H (decay length of the H) instead of R_Λ in Λ decay and R_Σ (decay length of Σ) instead of R_Ξ in Ξ^- decay.

As shown in Fig.8 and Fig.9, the detection efficiencies for the Σ^-, Λ and proton are consistent with unity if the flight length longer than 5 mm. On the basis of the above result,we fulfill the following requirement.

Requirement C: The decay lengths of the H and the Σ^- produced in the decay $H \rightarrow \Sigma^- p$ are longer than 5 mm. The flight length of the produced proton is also longer than 5 mm.

We have defined the detection efficiencies due to the following requirements D,E and F as η_o. The visibility is related to the angular resolutions of the tracks. Since we have set the minimum length to be 5 mm for each track the angular resolution σ_θ is 0.1 rad., which corresponds to the resolution of the opening angle of the kink to be 0.14 rad. We have required the angle between the Σ^- and the proton, $\theta_{\Sigma p}$, and the angle between the Σ^- and the π^-, $\theta_{\Sigma\pi}$, to be greater than $2\cdot\sigma_\theta$, $\sim$0.28 rad. for either projected plane, X-Z or Y-Z.

Requirement D: Both $\theta_{\Sigma p}$ and $\theta_{\Sigma\pi}$ are more than twice of the angular resolution, that is 0.28 rad.,in either of the X-Z or Y-Z plane.

To measure the three-dimensional positions of the initial and end points of tracks, we have required all the charged tracks to pass through at least 3 layers of fiber-sheets. It corresponds to the requirement for the flight lengths of Σ^-, proton and π^- along the direction of the beam axis to be longer than 1.5 mm.

Requirement E: Charged tracks are longer than 1.5 mm perpendicular to the layers of the scintillating-fiber-sheets.

As seen in Section 3, the overlapping of tracks of $H \rightarrow \Sigma^- p$ with the K^+ track or that with other beam tracks causes the inefficiency. To avoid the ambiguity due to overlap we require the following condition.

Requirement F: The distance between the K^+ track and the decay point of H is longer than 1 mm in either of the X-Z projection and the Y-Z projection.

4.3.3 Detection efficiency of "kinked Vee-track"

The overall detection efficiency of the scan is;

$$\eta_H = \eta_{P_K}(M_H) \times \eta_{decay}(M_H, \tau_H) \times \eta_{\pi out} \times \eta_{KV}(M_H, \tau_H), \tag{15}$$

where the η_{P_K} is the fraction of the events in which momentum of K^+ is above 1150 MeV/c^2. The η_{P_K} is about 0.95 for the total H production in the case of $M_H=2200$ MeV/c^2 and about 0.83 in the case of $M_H=2230$ MeV/c^2. The η_{decay} is a fraction of the events which satisfy Requirement A. It is determined by the lifetime of H and by that of Σ^-. The η_{decay} calculated by a Monte Carlo simulation is about 60% for H with the lifetime of 10^{-10}sec and about 30% for that with 10^{-9}sec. The $\eta_{\pi out}$ is a fraction of the events which satisfy Requirement B. The $\eta_{\pi out}$ is insensitive to M_H and τ_H due to the large Q-value of the decay $\Sigma^- \rightarrow \pi^- n$. It is 85% for the H with the mass of 2200 MeV/c^2 and the lifetime of 3×10^{-10}sec.

The $\eta_\Lambda(R_H, R_p) \times \eta_\Xi(R_\Sigma)$ is consistent with unity with Requirement C as discussed in Section 3. From the Monte Carlo study, about 30% of the H remains after Requirement C are fulfilled for the H's which have met Requirements A and B.

The efficiencies η_D, η_E and η_F due to Requirements D, E and F, respectively, have also been evaluated using a Monte Carlo simulation. These efficiencies discussed here are summarized in Table.6.

Table 6: The efficiencies of the cut according to Requirements A to F for the mass of 2200 MeV/c^2 and the lifetime of 3×10^{-10}sec. The values in the lower column show the efficiencies of the combined cuts. For example, the efficiency in the column "C" shows that of the combined cuts A to C.

Requirement	A	B	C	D	E	F	$P_{K^+}\geq$1150MeV/c
efficiency of each cut (%)	51.5	87.1	29.2	94.6	89.8	97.8	95.3
efficiency of combined cut (%)	51.5	44.8	13.1	12.4	11.2	10.9	10.4

The detection efficiency of H, η_H, which meets all the requirements A to F is shown in Fig. 12 as functions of the mass and the lifetime. The efficiency has highest value, that is, 11% for H with the mass of 2230 MeV/c^2 and the lifetime of 3×10^{-10} sec. It slightly decreases with increase of the H mass, whereas it is not so sensitive to the H mass.

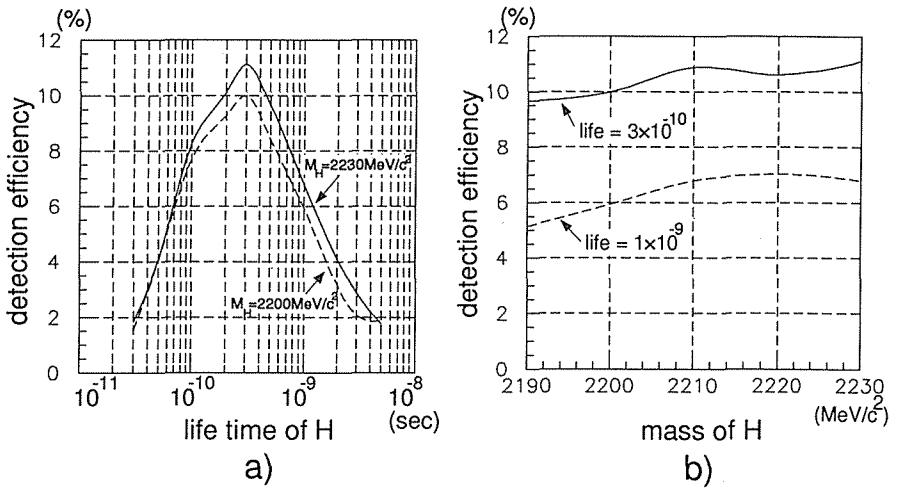

Fig. 12. The overall detection efficiency of the H decaying into $\Sigma^- p$. a) The efficiency as a function of the lifetime of H. The solid line shows the efficiency for $M_H = 2230$ MeV/c^2 and the dashed line for $M_H = 2200$ MeV/c^2. b) The overall efficiency as a function of the H mass for the cases that the τ_H is 3×10^{-10}sec and 3×10^{-9}sec,respectively.

4.3.4 Evaluation of the detection efficiency by scanning of the simulated pictures

We have examined the detection efficiency for the H by scanning simulated pictures of the $H \rightarrow \Sigma^- p$ decay like shown in Fig.11. In this sample, the lifetime of the H has been set to be 3×10^{-10}sec and the mass to be 2200 MeV/c^2. Also Requirements A and B has been fulfilled.

The correlation between R_H and R_Σ with $R_p \geq 5$ mm is shown in Fig.13. The closed circles show detected events which are scattered in the region where the track lengths are greater than 5 mm. The open circles correspond to the events which are not detected ones. One could find undetected events spread almost in the region where R_H and R_Σ are less than 5 mm.

After all the cuts from C to F have been performed, 44 events have been found,while 45 events have been expected from the detection efficiency described in the previous section. One event has not been found since the distance between the decay vertex of $H \rightarrow \Sigma^- p$ and the K^+ track is very close to the value required by F (2.3 mm in the X-Z picture and 0.9mm in the Y-Z picture). Thus we have concluded that the detection efficiency is almost 100% with Requirements A to F.

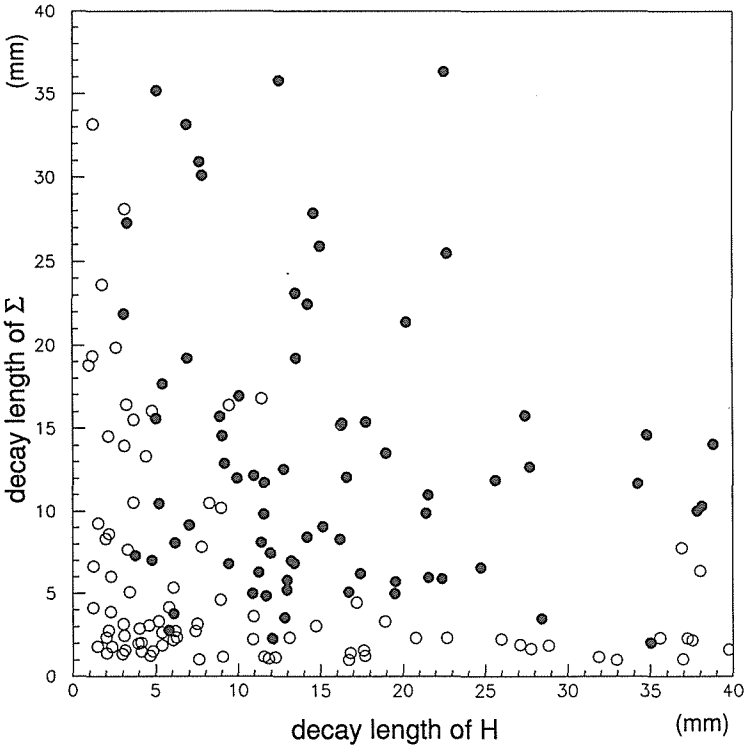

Fig. 13. The result of scanning of simulated pictures of H. The correlation between the decay length of the H and that of the Σ^- is shown with the condition of the proton flight length being greater than 5 mm. The closed circles have been found by scanning, while the open circles have not been found.

4.4 Analysis of $H \rightarrow \Sigma^- p$ candidates

Search for $H \rightarrow \Sigma^- p$ decay has been performed in the K^+ momentum region greater than 1150 MeV/*c*. The pictures of 697 events in this region have been scanned to find a "kinked Vee-track". First,we have carried out the cuts with Requirements A and B in order to search for the "kinked Vee-track"s from the event topologies. If the H is produced via the quasi-free process, no charged track is observed at the (K^-, K^+) vertex as discussed before. Nevertheless, we have not required any hypothesis for the topology of (K^-, K^+) vertex in this scanning in order to be free from unknown bias about the production mechanism.

After Requirements A and B, 6 events have remained. By Requirements C to F applied for these 6 events, 2 events are discarded, since one of the charged tracks in "Vee-track" has not passed through more than 4 sheets. The 4 events have been reconstructed as the final sample to be examined with the kinematical constraints of $H \rightarrow \Sigma^- p$ decay.

The pictures of the 4 events are shown in Fig.14. The reconstructions of the three-dimensional tracks have been done by the similar method as described in Section 3. The summary of the 4 events are listed in Table 7. The two events B and D are

associated with one prong at the (K^-, K^+) vertexes which can be interpreted as possible π^- emissions via Ξ^- decays with short decay length. However, we have adopted them as candidates for further tests with kinematical constraints.

Table 7: The summary of $H \rightarrow \Sigma^- p$ candidates. The values with asterisk show the visible energy with escaped proton.

event	A	B	C	D
K^+ momentum (MeV/c)	1189	1192	1169	1123
Number of prongs at (K^-, K^+) vertex	0	1	0	1
Opening angle for H decay (rad.)	1.69±0.26	1.10±0.16	2.44±0.12	1.59±0.07
Visible energy of proton (MeV)	26.9±3.6	29.5±2.7	37.1±2.1	73.4±1.3*
Visible energy of Σ^- (MeV)	83.6±6.8	75.5±1.6	50.1±2.0	63.8±2.8

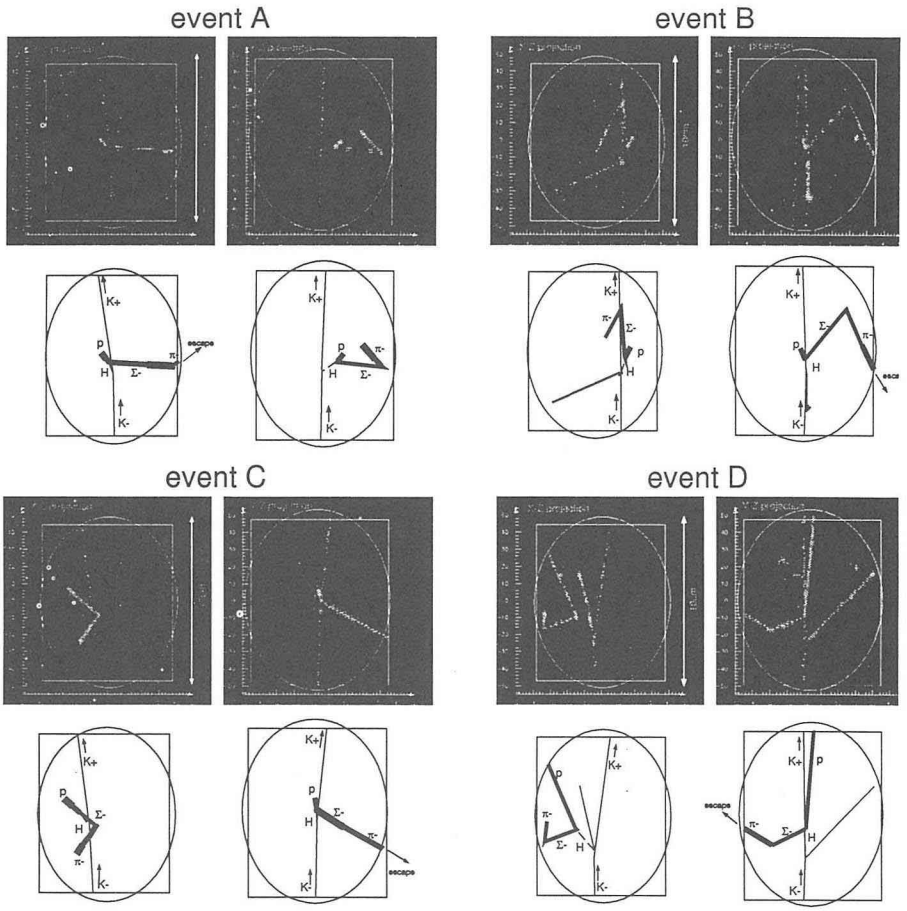

Fig. 14. Candidates of "kinked Vee-track". A possible interpretation for each event is shown under the respective picture.

There are several possibilities to "kinked Vee-track" faked by the decay products of Λ from Ξ^- decay at short distance or from Ξ^- interaction in the nucleus such as $\Xi^- p \rightarrow \Lambda\,\Lambda$. The first case is caused by the interaction of the proton or π^-. The second case is caused by the inflight decay of the π^- into μ^-. The probability of these cases has been estimated by using a Monte Carlo simulation. We have found that 0.55% of Λ's from Ξ^- decays fakes the "kinked Vee-track" due to the interaction of decay products, proton or π^-, and that 0.05% of the Λ's fakes due to $\pi^- \rightarrow \mu^- \bar{\nu}$ decay. Therefore, number of fake "kinked Vee-track" is expected to be 1.2 events from Λ's from Ξ^- at short distance. They are able to be eliminated by examination using the kinematics of the H decay as shown later. The third case, Λ interaction such as $\Lambda n \rightarrow \Sigma^- p$, is rather serious, but the momentum of Λ from (K^-, K^+) reaction is around 500 MeV/c which is lower than the threshold momentum, 670 MeV/c for this reaction. Assuming that cross section of the reaction $\Lambda + n \rightarrow \Sigma^- + p$ is about 100 mb, the probability of the reaction for Λ's from Ξ^- decays has been estimated to be less than 10^{-4}. We have found the fake events via the process is less than 0.02 events, which is negligibly small.

4.4.1 Kinematical constraints on the H candidates

We have examined the four candidates using kinematical constraints on the $H \rightarrow \Sigma^- p$ decay to separate from the background events. The first one is the "visible momentum" of the H which is reconstructed by using the ranges and the emission angles of the assumed Σ^- and proton. The minimum energy of a particle can be measured with its flight length in the SCIFI-target as described in Section 3. It is called "visible energy".

Table 8: a) The visible momentum of the H (P_H^{vis}) reconstructed from the visible energies of Σ^- and proton. b) The "visible momentum" of Λ (P_Λ^{vis}) obtained by the same method under the hypothesis that the $\Lambda \rightarrow p\,\pi^-$ decays produced "kinked Vee-track"s (see the text).

event	a) p_H^{vis} (MeV/c)	b) p_Λ^{vis} (MeV/c)
A	1343±242	266±120
B	1155±600	228±154
C	772±409	151±90
D	1926±261	378±73

The visible energy is equal to the kinetic energy of the particle if the particle stopped in the SCIFI-target. If particle decays or escapes from the target, the visible energy is smaller than the real kinetic energy. The visible energy of the Σ^-, T_Σ, is obtained as described in Section 3;

$$T_\Sigma = a(R_\Sigma)^b, \tag{16}$$

where R_Σ is the decay length of the Σ^-. The constant a and b are explained in Section 3. The visible momentum of Σ^-, p_Σ^{vis}, is obtained from T_Σ and the rest mass of the Σ^-, M_Σ as

$$p_{\Sigma}^{vis} = \sqrt{(T_{\Sigma} + M_{\Sigma})^2 - M_{\Sigma}^2}. \tag{17}$$

The visible momentum of H is obtained from P_{Σ}^{vis} , and the decay angles of the Σ^- and the proton, θ_{Σ}, θ_p as,

$$p_H^{vis} = p_{\Sigma}^{vis} \cdot (\cos\theta_{\Sigma} + \sin\theta_{\Sigma} / \tan\theta_p). \tag{18}$$

Table 9. The "visible momentum balance" for a) $H \rightarrow \Sigma^- p$ decay and b) $\Lambda \rightarrow p\,\pi^-$ decay.

event	a) Δp_H^{vis} (MeV/c)	b) Δp_{Λ}^{vis} (MeV/c)
A	-367 ± 91	-12 ± 62
B	-225 ± 65	20 ± 52
C	-215 ± 57	22 ± 45

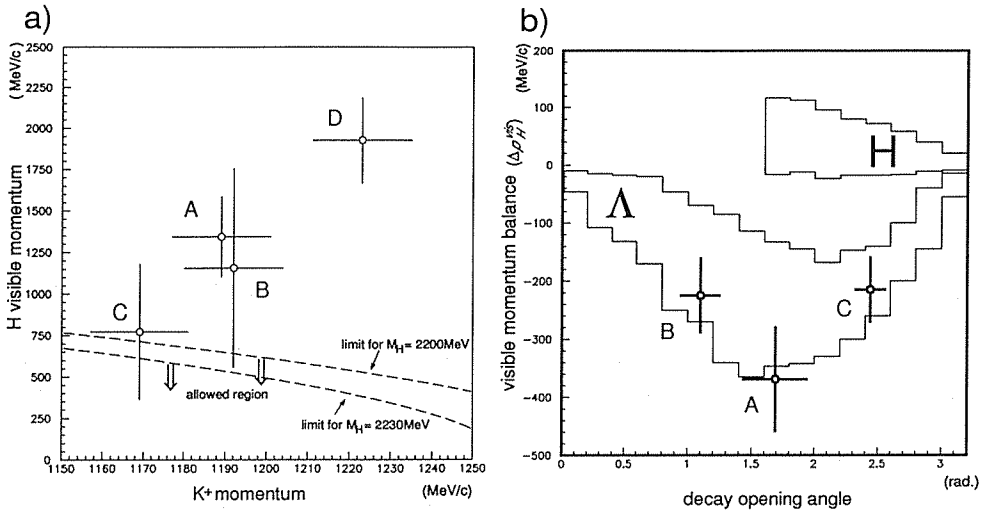

Fig. 15. a) The scatter plot of the visible momentum of the H and the momentum of K^+. The dashed lines correspond to kinematically allowed limits for the direct H production. Th upper line corresponds to the H mass of 2200 MeV/c^2 and the lower line to 2230 MeV/c^2. The areas below the dashed lines are allowed regions. b) The "visible momentum balance" is plotted against the decay opening angle. The area H and Λ show kinematically allowed regions which are derived from the Monte Carlo simulation. The area H corresponds to the decay $H \rightarrow \Sigma^- p$ with the H mass of 2230 MeV/c^2, and the area Λ corresponds to the decay $\Lambda \rightarrow p\,\pi^-$. The boundaries shown by the solid lines has 90% confidence level for the decays.

The visible momentum which is calculated by the same method with the hypothesis that the "kinked Vee-track" corresponds to the $\Lambda \rightarrow p\,\pi^-$ decay. The results of p_H^{vis} and p_{Λ}^{vis} are listed in Table 8. The p_{Σ}^{vis} for the events A, B, C, and D against the K^+ momentum are shown in Fig. 15-a). The dashed line shows the

kinematical limit of the momentum of H calculated for the following process which has the maximum Q-value;

$$K^- + {}^{12}C \rightarrow K^+ + {}^{10}B + H. \tag{19}$$

We have found that the two events A and D are inconsistent with the $H \rightarrow \Sigma^- p$ hypothesis. With the $\Lambda \rightarrow p\pi^-$ hypothesis, the visible momenta of the two events, A and D, are consistent with a typical momentum of Λ from (K^-,K^+) reaction.

The second constraint the "visible momentum balance" of the Σ^- and proton from the H decay. The visible momenta of the Σ^- and proton are obtained from their flight lengths;

$$p_\Sigma^{vis} = \sqrt{(T_\Sigma + M_\Sigma)^2 - M_\Sigma^2}, \tag{20}$$

$$p_p^{vis} = \sqrt{(T_p + M_p)^2 - M_p^2}, \tag{21}$$

where T_Σ and T_p are the visible energies of Σ^- and proton obtained from their flight lengths, respectively. The visible momentum balance, Δp_H^{vis} ,is defined as;

$$\Delta p_H^{vis} = p_p^{vis} \cdot \sin\theta_p - p_\Sigma^{vis} \cdot \sin\theta_\Sigma. \tag{22}$$

If the proton stops in the SCIFI-target, the Δp_H^{vis} should be a positive value, since the p_p^{vis} for the stopped proton is equal to the initial momentum, while the p_Σ^{vis} for the decaying Σ^- is always underestimated. The Δp_H^{vis} has been calculated for three events A,B and C in which protons have stopped in the SCIFI-target. The Δp_Λ^{vis} is the visible momentum balance which is calculated by the same method with the hypothesis of $\Lambda \rightarrow p\pi^-$. The results are listed in Table.9. The correlation between Δp_H^{vis} and the decay opening angle is shown in Fig 15-b). The region H and Λ show kinematically allowed region with 90% confidence level. The area H corresponds to the decay $H \rightarrow \Sigma^- p$, and the area Λ corresponds to the region due to $\Lambda \rightarrow p\pi^-$. The three events A, B and C are not consistent with the H but consistent with the Λ. By combining the kinematical constraints discussed above, we have concluded that all the 4 events A, B, C and D are fake events due to the Λ decays. Therefore, there remains no candidate of the $H \rightarrow \Sigma^- p$ decay.

5 Results and discussion

We have searched for the H in the decay products of the reaction, $K^- + C \rightarrow K^+ + H + X$, in the SCIFI-data. The "kinked Vee-track" topology corresponding to the sequential weak decay, $H \rightarrow \Sigma^- + p$ followed by $\Sigma^- \rightarrow \pi^- + \mathrm{p}$, has been searched for. Possible four candidates have been remained after scanning the SCIFI-data where the K^+ momentum is higher than 1150 MeV/c. We have rejected all the four events as the fakes of $\Lambda \rightarrow p\pi^-$ decay by means of the examination using the decay kinematics. From the null observed candidate the upper limit for the production cross section is obtained as;

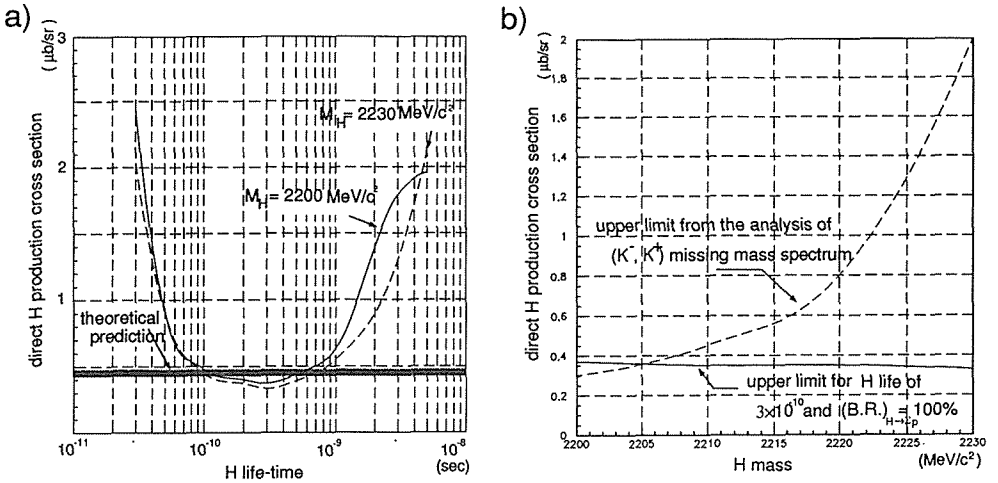

Fig. 16. The obtained upper limit for the cross section of the direct H production as a function of the lifetime is shown. The branching for the decay $H \to \Sigma^- p$ is assumed to be 100%. The solid line corresponds to $M_H = 2200$ MeV/c^2, and the dashed line corresponds to $M_H = 2230$ MeV/c^2. The straight line shows a theoretical prediction of the cross section. b) The upper limit for the cross section of the direct H production as a function of the mass of H with the lifetime of 3×10^{-10}sec is shown by the solid line. The branchings for the decay $H \to \Sigma^- p$ is assumed to be 100%. The dashed line shows the upper limit of the cross section deduced from only the missing mass spectrum of the (K^-, K^+) reaction (90% C.L.) obtained in this experiment in Ref.[42,44].

$$B_r \cdot \sigma_H \leq \frac{2.30}{N_{(K^-,K^+)} \cdot \eta_H} \cdot \sigma_{(K^-,K^+)}, \tag{23}$$

where Br is the decay branching for $H \to \Sigma^- p$. The η_H is the detection efficiency for the decay $H \to \Sigma^- p$ as described in Section 4.3. The upper limit for the σ_H depends on the mass and the lifetime of H. The $\sigma_{(K^-,K^+)}$ is the differential cross section of the (K^-, K^+) reaction at 0 degree on $(CH)_n$ target with $P_{K^+} \geq 950$ MeV/c. The absolute cross secton has been obtained for K^+ momentum greater than 950 MeV/c (8,294 events). The cross section of the (K^-, K^+) reaction has been taken from the experimental results in which the nuclear mass number dependence of the reaction was measured for various nuclear targets[36]. The 10% uncetainity of the measured cross section has not been included here. The possibilty that the produced Ξ^- escapes from the target nucleus[33] stops outside of the nucleus[34] and is absorbed in another nucleus is about 3% of the total (K^-, K^+) reactions. Therefore, our measurement includes the production of H through the process. However, it does not affect the final result of the upper limit for the direct H production cross section, because no candidate of the H production has been found. The results are shown as a function of the lifetime of H in Fig.16-a), and as a function of the H mass in Fig.16-b).

According to the prediction by Jaffe with the MIT bag model [2], the branching-

ratios of the H which decays into 2 baryons are expected as $\Sigma^- p : \Sigma^0 n : \Lambda n = 5:3:2$. If the H mass is greater than 2190 MeV/c^2, the decay $H \rightarrow \Lambda p \pi^-$ is also allowed. However, the branching of this decay is suppressed by the kinematical phase factor for the H mass near 2200 MeV/c^2.

It is difficult to assume the value of the branching ratio Br from the present theoretical works. Accordingly, the obtained upper limit is presented here assuming the branching ratio for the decay $H \rightarrow \Sigma^- p$ to be 100%. The upper limit is found to be to 0.3 μb to 0.5 μb with the H lifetime of 10^{-10}sec to 10^{-9} sec. The result is insensitive to the H mass in the region higher than 2200 MeV/c^2 as shown in Fig.16-a). The theoretical prediction using the method of Arts and Dover [18] is also shown in Fig.16-a). The obtained upper limit is of the same order as the predictions for the H with the lifetime of 10^{-10} to 10^{-9}sec and with assumption that the decay branching for $\Sigma^- p$ is 100%. The obtained upper limit is plotted as a function of the H mass for the lifetime of 3×10^{-10}sec in Fig.16-b). The direct H production in this mass region was also searched for by the analysis of the missing mass spectrum of (K^-, K^+) reaction in the experiment [34, 35] performed simultaneously with this experiment. It provided the upper limit without assumption of the decay branching-ratio of the H. The dashed curves in Fig.16-b) show the results.

The present results which have been obtained by searching the decay of H in the SCIFI-data put the new limit for the H near the $\Lambda\Lambda$ threshold (2200 MeV/$c^2 \leq M_H \leq$2230 MeV/c^2). It has been shown that the direct H production in this mass region is rejected by means of the analysis of missing mass spectrum as well as the searching for the decay products in the SCIFI-data.

6 Conclusion

The H dibaryon search via (K^-, K^+) reactions with the K^- momentum of 1.66 GeV/c has been performed at KEK 12-GeV Proton Synchrotron. In the present experiment a newly developed detector, SCIFI-target have been used as a visual detector in order to detect the image of (K^-, K^+) reactions followed by the H decay into $\Sigma^- p$ in the target. The K^+ -spectrometer which tags the (K^-, K^+) reactions has been used to confirm double strangeness transfer in the SCIFI-target. The SCIFI-target consists of 30,000 plastic scintillating fibers which are viewed by two sets of image intensifier tubes from the orthogonal directions providing three-dimensional information of the tracks. The tracks have been clearly identified as sequences of bright spots. The position resolution of the centroid of spot has been obtained to be 290 μm.

The H dibaryon through the direct production process, $K^- + C \rightarrow K^+ + H + X$ followed by the sequential weak-decay. $H \rightarrow \Sigma^- + p$, then $\Sigma^- \rightarrow \pi^- + n$, has been searched for in about 8,000 pictures of (K^-, K^+) reactions tagged with the K^+ -spectrometer having the momentum resolution of 0.5% and the mass resolution of 18.5 MeV/c^2 for K^+'s of 1.1 GeV/c.

The candidates of the possible H decays into $\Sigma^- p$ have been examined whether the decay kinematics are satisfied by the visible energy determined from the ranges of decay products. No candidate of the H decay has been found. The upper limit of

the production cross section of H decaying into $\Sigma^- p$ has been obtained to be 0.35 μb to 0.5 μb for the H with the mass of 2200 to 2230 MeV/c^2 and the lifetime of 10^{-10} to 10^{-9} sec.

The SCIFI-target has played important roles in this experiment owing to its unique feature as the triggerable visual detector. It has been worked as an active target providing three-dimensional information on (K^-, K^+) interaction vertexes, which has been used to reject background reactions such as neutral kaon productions. It has been also used to detect weak decay products of hyperons such as Ξ^-, Λ and the H produced via (K^-, K^+) reactions. In addition, the method of kinematical cuts has been successfully applied to separate the H decays from the background events due to Λ decays using the SCIFI-target.

In the present experiment the scintillating fiber has been used as an active target for the first time, and such a triggerable vertex detector has been proved to be useful, and the method for applying it to the scattering experiment has been established. Several kinds of experiments of hyperon-neucleon scattering has been performed and planned by using the SCIFI-target [37, 38, 39]. We believe that it will open a new field of particle and nuclear physics in future.

Acknowledgements

I would like to address my sincere thanks to Prof. Akira Masaike for his guidance and encouragement. I would like to express my thanks with grate respect to Prof. Ken'ichi Imai for various discussions with his keen insight for the physics. I would like to thank to Prof. Hideto En'yo for his powerful support and tireless devote to this work. I would express my gratitude to all the members of E224 collaboration. I would thank to S. Yamashita, M. S. Chung, Y. Goto, H. Funahashi, R. Takashima, M. Iinuma, P. Tlusty, M. Sekimoto, Y. Matsuyama, N. Saito, S. Makino, S. Yokkaichi, M. Yoshida, R. Susukita, S. Mihara, Y. Matsuda, A. Higashi, C. Nagoshi, and T. Fukuda for many precious contributions. I also would like to thank S. Aoki, T. Yoshida, T. Iijima, T. Nakano, F. Takeutchi, K. Omata and I. Nomura for the various supports and suggestions.

It is my pleasure to address grateful thanks to Prof. Y. M. Shin and Prof. K. S. Sim for giving us a good opportunity to work with many Korean physicists. Also thank to Korean collaborators, J. M. Lee, K. S. Chung, I. S. Park and J. K. Ahn for their devoted contributions and friendship.

This work was supported by many staffs of KEK. I explain thanks to Prof. K. Nakai,the head of the physics division of the KEK-PS for many supports and suggestions. I would thank to people of Beam Channel Group,M. Takasaki, K. Tanaka, Y. Yamanoi,especially to M. Ieiri for their hard works to maintain the beam line. I also would thank to people who supported the hardware and software for data taking, M. Nomachi, Y. Yasu, H. Kodama, T. Osuka, O. Sasaki for the various support.

I owe to express my acknowledgments to the companies, KURARY, Delft and HAMAMATSU for their powerful support to the present work. I would appreciate

to Japan Society of Promotion of Science for the financial support which helped the present work strongly.

References

[1] For detailed reviews, see Ann. Rev. Nucl. Part. Sci. **46** 332 (1990)
[2] R. L. Jaffe, Rev. Lett. **38**, 195(1977)
[3] P. J. Mulders, A. T. Aerts, and J. J. de Swart, Phys. Rev. **D21** (1980) 2653
[4] K. F. Liu and C. W. Womg, Phys. Lett. **113B** (1982)1.
[5] S. Takeuchi and M. Oka, Phys. Rev. Lett. **66** (1991) 1271.
[6] M. Oka, K. Shimizu and K. Yazaki, Nucl. Phys. **A464** (1987) 700.
[7] B. Sivestre-Brac, J. Carbonell and C. Gignoux, Phys. Rev. **D36** (1987) 2083.
[8] U. Straub, Z. Zhang, K. Bräuer, A. Faessler, S. B. Khadkikar and G.Lübeck, Nucl. Phys. **A508** (1990) 385c
[9] A. P. Balachandran, A. Barducci, F. Lizzi, V. G. J. Rodgers, and A. Stern, Phys. Rev. Lett. **52** (1984) 887.
[10] S. A. Yost and C. R. Nappi, Phys. Rev. **D32** (1985) 816.
[11] Y. Iwasaki, T. Yoshié and Y. Tsuboi, Phys. Rev. Lett. **60** (1988) 1371.
[12] A. S. Caroll et al., phys. Rev. Lett. **41** (1978) 777.
[13] A. M. Badalyan and Yu. A. Simonov, Sov. J. nucl. Phys.**36** (1982) 860.
[14] B. Shahbazian et al., Z. Phys **C39** (1988) 151.
[15] B. Shahbazian et al., Phys. Lett.**B316** (1993) 593.
[16] A. N. Alekseev st al., Sov. J. Nucl. Phys. **52** (1990) 1016.
[17] K. Jmai, Nucl. Phys. **A547** (1992) 199c-210c.
[18] A. T. M. Aerts and C. B. Dover, Phys. Rev. **D28**,450 (1983)
[19] A. T. M. Aerts and C. B. Dover, Phys. Rev. **D29**,433 (1984)
[20] S. Aoki et al., Phys. Rev. Lett.**65** (1990) 1729
[21] S. Aoki et al., (in preparation).
[22] S. Aoki et al., Prog. Theor. Phys. **85** (1991) 1287.
[23] J. K. Ahn et al., Nucl. Phys. **A547**(1992)211c-216c.
[24] A. R. Weindberg et al., Nucl Instr. Meth. **A283** (1989) 646.
[25] K. Kuroda et al., Nucl Instr. Meth.**A300** (1991) 259.
[26] P. Lendermann et al., Nucl Instr. Meth. **A344** (1994) 143.
[27] A. Cardini et al., Nucl. Instr. Meth. **A346** (1994) 163.
[28] A. Konaka et al., Nucl. Instr. Meth. **A256** (1987) 70.
[29] M. N. Atkinson et al., Nucl Instr. Meth. **A225** (1984) 1.
[30] M. N. Atkinson et al., Nucl Instr. Meth. **A263** (1988) 333.
[31] C. Angelini et al., Nucl Instr. Meth. **A277** (1989) 132.
[32] J. K. Ahn et al., Nucl Instr. Meth. (to be submitted).
[33] M. S. Chung, PhD thesis, Korea Univ. 1995, unpublished.
[34] S. Yamashita, *the Memoirs of the Faculty of Science, Kyoto University, Series A of Physics, Astrophysics, Geophysics and Chemistry,* 1995 (to be published), PhD thesis Kyoto Univ. 1995, unpublished.
[35] J. K. Ahn et al., Phys. Rev. Lett. (to be submitted).
[36] T. Iijima et al., Nucl. Phys. **A546** (1992) 588.
[37] KEK E251 experiment, M. Ieiri et al.
[38] KEK E289 experiment, M. Ieiri et al.
[39] BNL E885 experiment.